scientific reports

Check for updates

OPEN

MiR-485-3p/MELK cascade mediates tumor progression in pancreatic cancer

Yishan Huang[1], Ting Yang[1], Chen Yang[1], Bo Tang[2], Bo Su[3]✉ & Xiaojun Yang[1,4]✉

Pancreatic cancer remains one of the leading causes of mortality worldwide, largely due to the limitations of current clinical strategies for its treatment. As a result, identifying genetic alterations and potential therapeutic targets could offer new opportunities for improving the diagnosis and treatment of pancreatic cancer. The identification of differentially expressed genes (DEGs) and subsequent analyses, including signaling pathway enrichment, functional classification, and protein-protein interaction (PPI) network construction, were conducted using three public datasets: GSE32676, GSE71989, and GSE16515. Kaplan-Meier survival curves and receiver operating characteristic (ROC) curves were employed to investigate the correlation between hub genes and clinicopathological features in pancreatic cancer patients. Genetic alterations were analyzed using the CBioPortal web tool. Cell proliferation was assessed through CCK-8, colony formation, and EdU assays. Tumor migration, invasion, and angiogenesis were evaluated using transwell and tube formation assays, respectively. Protein and mRNA expression levels were measured via western blot analysis and qPCR assays. The subcutaneous xenografted nude mice models were generated to evaluate the potential effect of miR-485-3p/MELK cascade on tumor growth in vivo. Our analysis revealed that MELK expression is positively correlated with poor prognosis in patients with pancreatic cancer. The overexpression or knockdown of MELK significantly influences cell proliferation, tumor metastasis, and angiogenesis across various pancreatic cancer cell lines. Furthermore, we identified that miR-485-3p regulates MELK expression by directly targeting the *MELK 3'UTR* binding site in pancreatic cancer cells, which subsequently impacts tumor progression. Additionally, our findings demonstrate that the miR-485-3p/MELK cascade is closely associated with tumor progression in pancreatic cancer cells. Mechanistically, the miR-485-3p/MELK cascade promotes the phosphorylation of Akt to regulate pancreatic cancer cell progression, metastasis, and angiogenesis. Furthermore, overexpression of miR-485-3p inhibits the tumor growth induced by MELK overexpression in subcutaneous xenograft model. MiR-485-3p/MELK cascade may serve as a promising biomarker and therapeutic target for the diagnosis and treatment of pancreatic cancer.

Keywords MELK, miR-485-3p, Tumor progression, Pancreatic cancer, Biomarker

Pancreatic cancer (PC) is one of the most lethal forms of malignant cancer, characterized by high mortality rates and poor prognoses[1]. According to GLOBOCAN 2022, there were 510,566 newly diagnosed cases of pancreatic cancer and 467,005 associated deaths, with an approximate 5-year survival rate of just 7%[2]. By 2030, pancreatic cancer is projected to become the second leading cause of cancer-related deaths, with one of the highest incidence rates among malignant cancers[3]. Surgical resection, combined with subsequent chemo-radiotherapy, remains the only potentially curative treatment for improving the prognosis of pancreatic cancer patients[4]. However, prognostic outcomes continue to be poor due to the limitations of current therapeutic approaches. Consequently, the identification of potential therapeutic targets, which could significantly enhance diagnostic accuracy and prognostic prediction, may prove instrumental in advancing clinical treatment options for pancreatic cancer.

Maternal embryonic leucine zipper kinase (MELK) is a Ser/Thr protein kinase, also known as a cell cycle-dependent protein kinase, and is categorized as an atypical member of the Snf1/AMPK family[5–7]. Previous

[1]Engineering Research Center of Key Technique for Biotherapy of Guangdong Province, Shantou University Medical College, Shantou 515041, China. [2]Department of Hepatobiliary Surgery, The First Affiliated Hospital of Guangxi Medical University, Nanning 530021, China. [3]Department of Cell Biology, School of Basic Medical Science, Shandong University, Jinan 250012, China. [4]The First Dongguan Affiliated Hospital, Guangdong Provincial Key Laboratory of Medical Molecular Diagnostics, School of Basic Medicine, Guangdong Medical University, Dongguan 523808, China. ✉email: bxs103@sdu.edu.cn; yangx@stu.edu.cn

studies have reported that MELK is highly expressed in various malignant tumors, including breast, prostate, gastric, and cervical cancers[8–11], suggesting its significant role in tumor progression[12]. Importantly, further research has revealed that MELK mediates multiple biological events and signaling pathways to regulate various tumor-associated processes, such as cell cycle progression, cell proliferation, apoptosis, tumor metastasis, and chemotherapy resistance[13–15]. Notably, MELK functions as a novel oncogenic regulator by directly interacting with other factors or activating phosphorylation in these processes. For instance, one study demonstrated that MELK, as an upstream kinase of apoptosis signal-regulating kinase 1 (ASK1), interacts with ASK1 to phosphorylate threonine 838 and enhance ASK1's kinase activity[16]. Another report revealed that MELK inhibits breast cancer cell apoptosis by directly binding to Bcl-G, a pro-apoptotic member of the Bcl-2 family[8]. Additionally, MELK has been shown to promote cell cycle arrest and apoptosis by interacting with the p53 protein through direct phosphorylation at the Ser15 site[17]. The elevated expression of MELK in various tumors underscores its critical role in tumor progression while highlighting its potential as a therapeutic target for cancer treatment. Nonetheless, the specific functions of MELK in the progression of pancreatic cancer remain insufficiently studied.

In this study, we initially identified MELK using bioinformatics techniques, which included analyzing differentially expressed genes (DEGs), performing functional enrichment analysis, and constructing a protein-protein interaction (PPI) network for pancreatic cancer. The findings demonstrated that MELK is highly expressed in pancreatic cancer, suggesting it could serve as an independent molecular prognostic factor for patients with this disease. Furthermore, we investigated the potential role of MELK in pancreatic cancer cells. Our results indicated that overexpression of MELK significantly enhances the proliferation, invasion, metastasis, and angiogenesis of these cells. Additional research uncovered that miR-485-3p functions as an upstream regulator of MELK and suppresses pancreatic cancer progression by modulating MELK expression. Collectively, our findings suggest that MELK could be a promising biomarker for predicting the prognosis of pancreatic cancer patients and may offer a potential strategy for treating this condition.

Materials and methods

Public database

The microarray gene expression datasets, including GSE32676, GSE71989, and GSE16515, were downloaded from the Gene Expression Omnibus (GEO) database (https://www.ncbi.nlm.nih.gov/)[18]. All three datasets were generated using the same platform, the Affymetrix Human Genome U133 Plus 2.0 Array (HG U133 Plus 2.0). Specifically, the GSE32676 dataset includes 25 samples from human pancreatic cancer tissues and 7 samples from adjacent normal tissues. Similarly, the GSE71989 dataset comprises 14 pancreatic cancer samples and 8 adjacent normal pancreatic tissue samples, while the GSE16515 dataset consists of 36 pancreatic tumor samples and 16 adjacent normal samples. The distribution of data for each sample is visualized using box plots. The effectiveness of batch effect correction is evaluated through principal component analysis (PCA) and uniform manifold approximation and projection (UMAP) plots. These visualizations were created using R software with the `ggplot2` package.

The identification of differentially expressed genes (DEGs)

Differential gene expression in pancreatic cancer samples was analyzed using the GEO2R web tool available on the NCBI Gene Expression Omnibus (https://www.ncbi.nlm.nih.gov/). The DEGs were identified based on the following screening criteria: $|\log(FC)| > 1$ and $P < 0.05$. The R package `ggplot2` was utilized to generate the volcano plots, while the heatmap was created using the `pheatmap` software package. Overlapping genes were identified with the help of the Venn online tool, available at http://bioinformatics.psb.ugent.be/webtools/Venn/ .

Kyoto encyclopaedia of genes and genomes (KEGG) and gene ontology (GO) enrichment analyses

The KEGG and GO enrichment analyses of differentially expressed genes (DEGs) were conducted using the DAVID Gene Ontology Functional Annotation Tool. GO terms are categorized into three groups: Biological Process (BP), Molecular Function (MF), and Cellular Component (CC). The bubble plots were visualized using ggplot2. A *P*-value of less than 0.05 was considered statistically significant. The KEGG (Kyoto Encyclopedia of Genes and Genomes) (https://www.genome.jp/kegg/) enrichment, a comprehensive website including an extensive array of biochemistry pathways[19–21], were performed using KEGG database.

PPI network construction and hub genes identification

The STRING database encompasses data on over 2,000 organisms and employs innovative, scalable algorithms to relay information about interactions among these organisms[22]. It was leveraged to predict interactions between known and predicted proteins. Using the STRING database, a protein-protein interaction network was constructed for the DEGs. A minimum required score of 0.4 was set as the threshold. Hub genes were subsequently identified through Cytoscape 3.7.1 software with the help of the cytoHubba plugin.

The prognostic analyses of hub genes in pancreatic cancer

Gene expression data for hub genes across 33 tumor types were sourced from the Cancer Genome Atlas (TCGA, available at https://portal.gdc.cancer.gov/). The mRNA expression of these hub genes in both the tumors and normal samples was analyzed using the TCGA database. Kaplan-Meier curves were generated to conduct survival analysis, utilizing the R 'survival' package. This package facilitates Kaplan-Meier analysis with log-rank testing, which was employed to analyze survival data. Visualization was carried out with the R package 'ggplot2'.

Additionally, the receiver operating characteristic (ROC) curve analysis was performed using the ROC function of an R package.

Univariate and Multivariate Cox regression analyses were conducted to explore the relationship between prognosis and the expression of hub genes as well as clinicopathological parameters. A nomogram was developed to predict associations between risk factors, including clinicopathological parameters and gene expression, and disease outcomes. The model's accuracy was quantified using the C-index, while its performance was further validated through calibration plots.

Mutation analyses

The cBioPortal (http://cbioportal.org) is an online database that consolidates data from a variety of cancer genomics studies. The integrated genomic data types encompass somatic mutations, DNA copy number alterations (CNAs), mRNA and microRNA (miRNA) expression, DNA methylation, and protein abundance[23]. Using the cBioPortal database, the mutation frequencies of MELK in pancreatic cancer were systematically analyzed.

Cell culture, treatment, and transfection

The human pancreatic cell lines, PANC-1 and AsPC-1, were obtained from the China Center for Type Culture Collection in Wuhan, China. PANC-1 cells were cultured in Dulbecco's Modified Eagle's Medium (Corning, VA), while AsPC-1 cells were maintained in RPMI-1640 Medium (Corning, NY). Each culture medium was enriched with 10% fetal bovine serum (FBS, Yeasen, Shanghai, China) and a 1% penicillin-streptomycin antibiotic solution (Yeasen). All cells were incubated in a humidified environment at 37 °C with 5% CO_2. The Akt inhibitors (Capivasertib; HY-15431) was obtained from MedChem Express (Monmouth Junction, NJ) and the different groups of cells were treated with capivasertib (10 μM) for 48 h before the following experiments.

For cell transfection, the recombinant plasmid designed to overexpress MELK was procured from VectorBuilder (Guangzhou, China). The miR-485-3p mimic, inhibitor, and their corresponding control plasmids (NC mimic and NC inhibitor) were synthesized by RiBo Biotech (Guangzhou, China). Transfection was performed using Lipofectamine 3000 reagent (Invitrogen, Thermo Fisher Scientific, Waltham, MA) accordance with the manufacturer's protocol.

Quantitative real-time PCR (qRT-PCR) assay

Total RNA was extracted from pancreatic cancer cells using the TRIzol reagent (Invitrogen). This RNA was then reverse transcribed using the Mir-XTM miRNA First-Strand Synthesis Kit (TaKaRa Bio, Japan). Quantitative PCR (qPCR) was conducted with the SYBR Green PCR Master Mix (GenStar, Beijing, China). miRNA levels were quantified utilizing the CFX Connect Real-Time PCR Detection System and CFX Manager Software (Bio-Rad). The data were analyzed with the 2-ΔΔCt method, and miR-485-3p expression was normalized using U6 as an internal reference. The primers used included the miR-485-3p forward primer (5'-GTCATACACGGCTC TCCTCTCT-3'), the reverse primer provided by the Reverse Transcription Kit, the U6 forward primer (5'-GGA ACGATACAGAGAAGATTAGC-3'), and the reverse primer (5'-TGGAACGCTTCACGAATTTGCG-3'). The experiments were conducted in triplicate.

Western blotting analysis

Protein samples were extracted using RIPA lysis buffer (Yeasen), and protein concentrations were measured with the BCA Protein Assay. The samples were resolved via 12% SDS-PAGE and subsequently transferred onto PVDF membranes (Millipore, Billerica, MA). The membranes were blocked with 5% BSA in TBST solution (1% Triton X-100 in PBS) for 1 h at room temperature. Following blocking, the membranes were washed with TBST buffer and incubated overnight at 4 °C with primary antibodies.

All primary antibodies were sourced from the Proteintech Group (Rosemont, IL) and included the following: mouse anti-human CyclinD1 monoclonal antibody (mAb; 60186-1, 1:1000), rabbit anti-human MMP2 mAb (10373-2-AP, 1:1000), rabbit anti-human MMP9 mAb (30592-1-AP, 1:1000), rabbit anti-human VEGFA mAb (19003-1-AP, 1:2000), rabbit anti-human phospho-Akt mAb (28731-1-AP, 1:1000), rabbit anti-human Akt mAb (10176-2-AP, 1:1000), rabbit anti-human phospho-β-Catenin (AP0979, 1:1000), rabbit anti-human β-Catenin mAb (A19657, 1:1000), and rabbit anti-human GAPDH mAb (10494-1-AP, 1:5000). After additional washes with TBST solution, the membranes were incubated with either an anti-rabbit HRP-conjugated secondary antibody (SA00001-2, 1:5000) or an anti-mouse HRP-conjugated secondary antibody (SA00001-1, 1:5000). Chemiluminescence signals were developed using ECL reagent (Yeasen), and pixel intensities were quantified with ImageJ software (National Institutes of Health, Bethesda, MD). Each experiment was performed in triplicate.

Cell counting kit-8 (CCK-8) assay

The cell viability was assessed using the CCK-8 assay. Pancreatic cells from different groups were seeded into 96-well plates at a density of 3×10^3 cells per well. Subsequently, 10 μL of CCK-8 reagent (Dojindo, Japan) was added to each well, and the cells were incubated at 37 °C for 2 h. Absorbance was then measured at 450 nm using a Multi-Mode Microplate Reader (BioTek Instruments, Winooski, VT). The experiments were determined with three replicates.

Colony formation assay

The distinct groups of pancreatic cells (1×10^3 cells per well) were subjected to full trypsinization and seeded into a 6-well plate. The cells were subsequently cultured for a duration of 2 or 3 weeks. Following this period, the culture medium was carefully removed, and the wells were rinsed three times with PBS solution. The cells were

then fixed using 4% paraformaldehyde (PFA) and stained with crystal violet for 20 min. Finally, the total number of colonies was quantified using ImageJ software. The experiments were determined with three replicates.

EdU assay

The various groups of transfected PANC-1 and AsPC-1 cells were cultured overnight in a 12-well plate, with each well containing 1×10^4 cells. Subsequently, EdU reagent (Beyotime, Shanghai, China) was added to the culture medium, achieving a final concentration of 10 μM. The cells were incubated at 37 °C for four hours, then fixed with 4% PFA and permeabilized in a PBS solution containing 0.3% Triton X-100 for 10 min at room temperature. A volume of 250 μl of reaction solution was added to each well, followed by a 30-minute incubation at 37 °C. After washing with PBS solution, the nuclei were stained with Hoechst 33,342 (Life Technologies, Thermo Fisher Scientific). Images were captured using an Axio Observer A1 microscope (Carl Zeiss, Germany). The experiments were determined with three replicates.

Transwell assay

To assess cell migration and invasion capabilities, cell culture inserts—either coated with Matrigel (BD Biosciences, San Jose, CA) for invasion assays or uncoated for migration assays—were placed into 6-well plates. A total of 7×10^4 PANC-1 and AsPC-1 cells from different experimental groups were seeded into the upper chamber of the inserts using serum-free DMEM medium. Meanwhile, 600 μl of culture medium containing 10% FBS was added to the bottom chamber. After 16 h of incubation, cells remaining on the upper surface of the membranes were carefully removed with a cotton swab. The membranes were then fixed with 4% formaldehyde and stained with 0.1% crystal violet. The number of migrated and invaded cells was counted under a microscope and quantified using ImageJ software. The experiment were determined with three replicates.

Tube formation

The ice-cold Matrigel (50 μl per well) was carefully added to a 96-well plate and incubated at 37 °C for 30 min to allow solidification. Suspended cells (4×10^4 cells per well) from various groups were then seeded into the solidified Matrigel within the 96-well plate and cultured for 6 h. Images were captured using a Zeiss Axiovert 200 M microscope (Zeiss, Germany) and analyzed with ImageJ software. Each experiment was performed in triplicate.

Luciferase assay

To determine whether miR-485-3p directly targets the MELK 3'UTR, the normal control and mutated miR-485-3p binding sites within the MELK 3'UTR were cloned into a pGL6 vector (Invitrogen). These constructs contain NC mimic (NC) and miR-485-3p mimic (miR-485-3p) were subsequently transfected into PANC-1 and AsPC-1 cells using Lipofectamine 3000. Following a 48-hour incubation period, luciferase activities were assessed using a Dual Luciferase Reporter Gene Assay Kit (Beyotime) in accordance with the manufacturer's instructions.

Quantification and statistical analyses

All statistical analyses were conducted using R software (Version 4.1.2) and GraphPad Prism 8.0 (GraphPad Software, San Diego, CA). Each experiment was performed at least three times. Data are presented as mean ± SEM. The ROC curve was generated using the pROC package, while differences between Kaplan-Meier survival curves were evaluated using the log-rank test. Statistical analysis of gene-gene correlations was carried out through Pearson correlation. For comparisons between two groups, a two-tailed unpaired Student's *t*-test was employed. Differences among three or more groups were analyzed using one-way ANOVA, followed by Tukey's multiple comparisons test. A *P*-value of less than 0.05 was considered statistically significant.

Animals and tumor xenograft model

The 6 week male BALB/c-nude mice were obtained from GemPharmatech Company (Foshan, China, animal license no. SCXK 2023-0067). All experimental procedures were conducted in accordance with the approval and guidelines of the Animal Care Committee of Shantou University Medical College (SUMCSY2025-003). This study involving animals are reported in accordance with the ARRIVE guidelines. The mice were housed in the specific-pathogen free environment with temperature 24–28 °C under a 12-h dark/light cycle with free access to food and water. MELK overexpressing and vehicle control PANC-1 (1×10^7) or AsPC-1 (6×10^6) cells were subcutaneously inoculated into the left forelimb of BALB/c nude mice ($n = 4$ or $n = 6$ for each group) in 200 μL of a 1:1 mixture of PBS/Matrigel. When the tumor volume reached 50–100 mm^3, miR-485-3p agomiR and agomiR NC (10 nmol / 50 μL) were then intratumorally injected into the mice every 2 days for 2 consecutive weeks. Tumor sizes were measured every 3 or 4 days with a vernier caliper, and tumor volume was calculated according to the following formula: volume = 0.5 × length × $width^2$.

Results

The analyses of DEGs, signaling pathway enrichment, functional classification, and PPI network in pancreatic cancer

To systematically explore aberrant gene expression in pancreatic cancer, three gene expression datasets from the GEO database contains GSE32676, GSE71989, and GSE16515, were analyzed to compare differential gene expression (DEGs) between pancreatic cancer tissues and adjacent normal tissues. Following normalization of the expression matrices for these datasets, boxplots revealed that the medians of each subgroup aligned closely along the same straight line (Fig. 1A-C). Notably, principal component analysis (PCA) (Fig. 1D-F) and uniform manifold approximation and projection (UMAP) plots (Fig. 1G-I) indicated a clear distinction between pancreatic cancer samples and the control group. Subsequently, DEGs were identified based on the criteria of

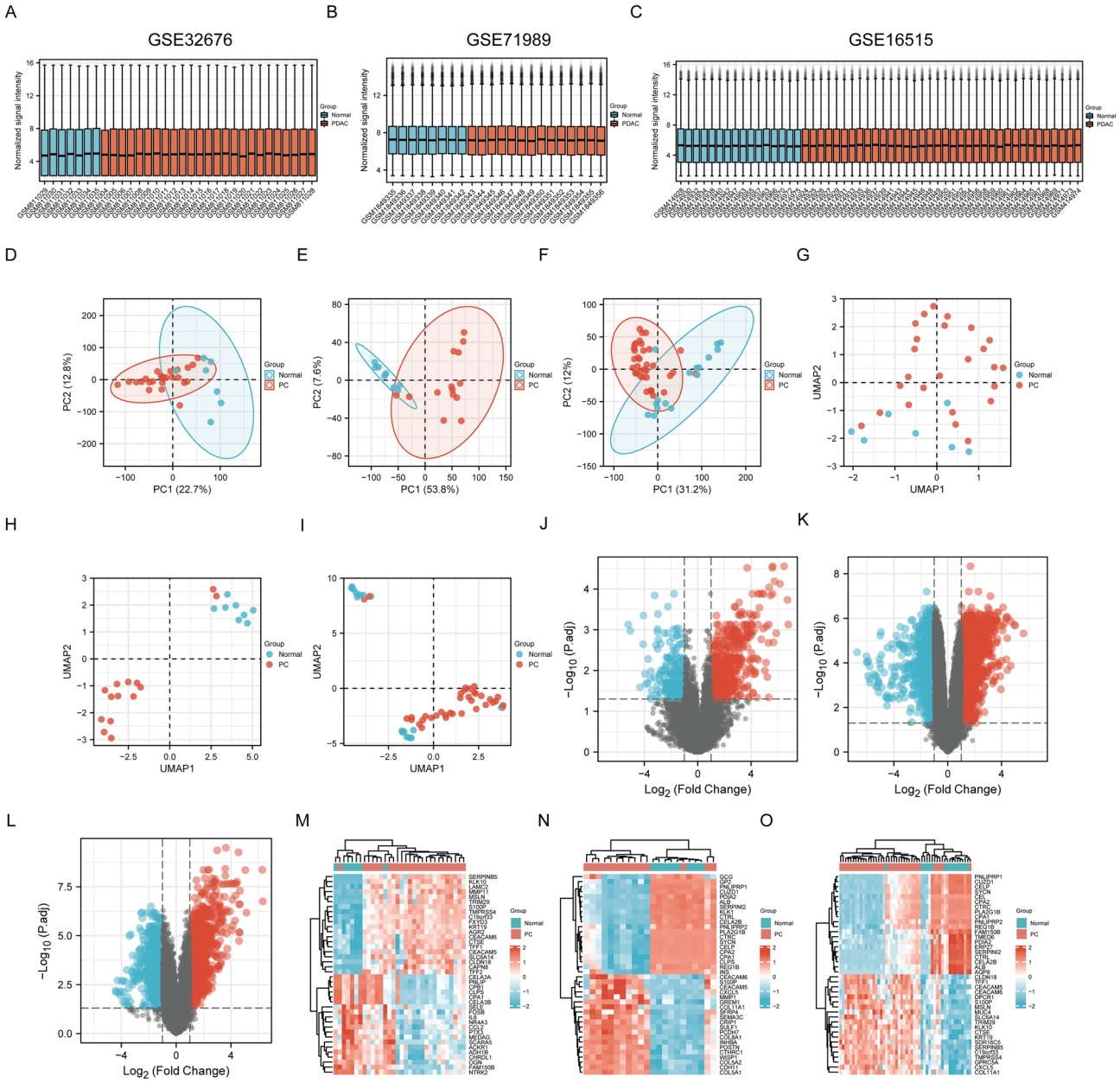

Fig. 1. Identification of DEGs in pancreatic cancer from GSE32676, GSE71989, and GSE16515 datasets. (**A-C**) Box plots display the sample distribution and median values for the GSE32676, GSE71989, and GSE16515 datasets, respectively. (**D-F**) Principal Component Analysis (PCA) plots depict the distribution of normal and pancreatic cancer groups across the three datasets. Blue squares represent the normal groups; red circles represent the pancreatic cancer groups. (**G-I**) Uniform Manifold Approximation and Projection (UMAP) plots illustrate the delineated clusters within the three datasets. Blue squares correspond to the normal groups; red circles correspond to the pancreatic cancer groups. (**J-L**) Volcano plots highlight the DEGs in the datasets. Blue indicates downregulated genes, red indicates upregulated genes, while gray represents genes with no significant changes. (**M-O**) Heatmaps showcase the top 20 upregulated and downregulated DEGs in the GSE32676, GSE71989, and GSE16515 datasets, respectively. DEGs, diferentially expressed genes; PCA, principal component analysis; UMAP, uniform manifold approximation and projection; PC, pancreatic cancer.

$|\log(FC)| > 1$ and $P < 0.05$. The analysis detected 749 DEGs (509 upregulated and 240 downregulated genes) in GSE32676, 2839 DEGs (1801 upregulated and 1038 downregulated genes) in GSE71989, and 1483 DEGs (951 upregulated and 532 downregulated genes) in GSE16515 (Fig. 1J-L). Among these DEGs, heatmaps highlighting the top 40 genes, including the top 20 upregulated and top 20 downregulated genes, were constructed for pancreatic cancer in each of the three GEO datasets (Fig. 1M-O).

We next conducted KEGG enrichment analysis to identify potential downstream signaling pathways associated with the differentially expressed genes (DEGs) in pancreatic cancer. The results revealed that the

significant KEGG signaling pathways in the three datasets were primarily enriched in the PI3K/Akt signaling pathway, malaria, ECM-receptor interaction, tight junction, pathogenic Escherichia coli infection, phagosome, focal adhesion, viral myocarditis, protein digestion and absorption, mineral absorption, pancreatic secretion, and glycolysis/gluconeogenesis pathways, respectively (Fig. 2A-C, Supplementary Tables 1–3). Additionally, further analysis of Gene Ontology (GO) biological processes, encompassing BP (biological process), MF (molecular function), and CC (cellular component) categories, showed that the key processes were mainly enriched in cell junction organization, cell junction assembly, cell-cell junction organization, urogenital system development, cell-cell junctions, the apical part of the cell, apical plasma membrane, apical junction complex, cell adhesion molecule binding, actin binding, cadherin binding, and cell adhesion mediator activity across all three pancreatic cancer datasets (Fig. 2D-F, Supplementary Tables 4–6). These findings suggest that the identified pathways and biological functions play critical roles in pancreatic cancer tumor progression.

After identifying the 161 overlapping DEGs from the three datasets analyzed using Upsetplot and Venn diagram (Fig. 2G, H), subsequent KEGG enrichment analysis revealed that these overlapping DEGs were primarily associated with pathways such as human papillomavirus infection, ECM-receptor interaction, salivary secretion, the p53 signaling pathway, and mucin-type O-glycan biosynthesis (Fig. 2I). Moreover, GO analysis highlighted that the DEGs were linked to processes and components including response to metal ions, cell junction assembly, keratinocyte proliferation, hemidesmosome assembly, and the collagen-containing extracellular matrix. Additionally, they were associated with the midbody, secretory granule lumen, laminin complex, cell adhesion molecule binding, enzyme inhibitor activity, extracellular matrix binding, and laminin binding in pancreatic cancer (Fig. 2J).

To further illustrate the roles of the 161 overlapping DEGs in pancreatic cancer, we constructed a PPI network using the STRING database (Fig. 2K). Through hub gene identification and module analysis of the PPI network using the MCODE plugin in Cytoscape, we identified the top 10 hub DEGs (represented as red dots in Fig. 2L): *MELK*, *CEP55*, *NUSAP1*, *ASPM*, *CDK1*, *RRM2*, *TOP2A*, *CENPF*, *PRC1*, and *PBK*. Additionally, we analyzed the expression of these identified hub DEGs across various cancers using the TCGA and GTEx databases. As anticipated, the expression of these hub genes was significantly altered in the majority of malignant tumors (Supplementary Fig. 1A-J). Notably, the findings also revealed that all these hub genes were highly expressed in pancreatic cancer compared to normal tissues (Supplementary Fig. 1K-T), suggesting that these genes may play critical roles in the development and progression of pancreatic cancer.

MELK expression are positive correlative to the prognosis of pancreatic cancer

To determine whether the expression of these hub genes is critical for predicting the prognosis of pancreatic cancer, we examined their correlation with patient outcomes. Kaplan-Meier analysis demonstrated that the expression of all these hub DEGs was associated with poor prognosis in pancreatic cancer patients (Supplementary Fig. 2A-J). Furthermore, additional ROC analysis showed that the areas under the ROC curve for all these genes were significantly greater than 0.9 (Supplementary Fig. 2K-T), highlighting their potential as biomarkers for predicting pancreatic cancer prognosis.

We investigated the correlation between these hub genes and clinical features, such as age, gender, pTNM stage, grade, radiation therapy, and prognosis, by using univariate and multivariate Cox regression analyses. Through univariate Cox regression analysis, we found that all hub genes except *NUSAP1*, along with the clinical features, including age, grade, and radiation therapy, were significantly associated with the poor prognosis of pancreatic cancer patients (Fig. 3A). Notably, multivariate Cox regression analysis identified several significant risk factors, including age, grade, radiation therapy, and MELK expression, which could serve as potential predictors of prognosis. Among these, MELK expression emerged as an independent prognostic factor for predicting outcomes in pancreatic cancer patients (Fig. 3B). Based on the results of the multivariate Cox regression analysis, a nomogram was constructed to predict 1-, 3-, and 5-year overall survival (OS) for pancreatic cancer patients, using the identified prognostic factors (Fig. 3C). Calibration curves were employed to evaluate the predictive accuracy of the nomogram model, and the curves demonstrated excellent agreement with observed OS outcomes at 1, 3, and 5 years (Fig. 3D). Further prognostic analyses revealed a strong positive correlation between high MELK expression and poor pancreatic cancer prognosis across multiple metrics, including OS, progression-free survival (PFS), disease-specific survival (DSS), and disease-free interval (DFI) (Fig. 3E–H). These findings suggest that MELK expression may play a crucial role in the progression of pancreatic cancer.

Mutation signature and DEGs enrichment analyses of MELK in pancreatic cancer

To better understand the mutational signature and biological role of MELK in tumor progression, we utilized the cBioPortal platform to analyze mutation frequencies in pancreatic cancer patients. The analysis revealed a notable frequency of MELK mutations, exceeding 10%, in pancreatic cancer (Fig. 4A). The predominant mutation type observed in MELK was identified as mRNA mutations, and the schematic representations of protein domain information and mark mutation positions of MELK were visualized through lollipop plots (Fig. 4B and C).

To investigate the potential biological roles of MELK in pancreatic cancer, we conducted GO term enrichment analysis to identify the DEGs influenced by aberrant MELK expression. The GO analysis revealed that these DEGs were predominantly enriched in pathways related to the cell cycle, oocyte meiosis, cell motility, cell adhesion, and DNA replication (Fig. 4D). Heatmaps highlighted the top 10 DEGs associated with aberrant MELK expression in pancreatic cancer, including *CDK1*, *ORC6*, *SPAG5*, *CEP55*, *ZWINT*, *TPX2*, *KIF4A*, *HJURP*, *NCAPG*, and *NCAPH* (Fig. 4E). Furthermore, correlation analyses demonstrated that the mRNA expression levels of these key genes were positively correlated with MELK expression in pancreatic cancer (Figs. 4F–O).

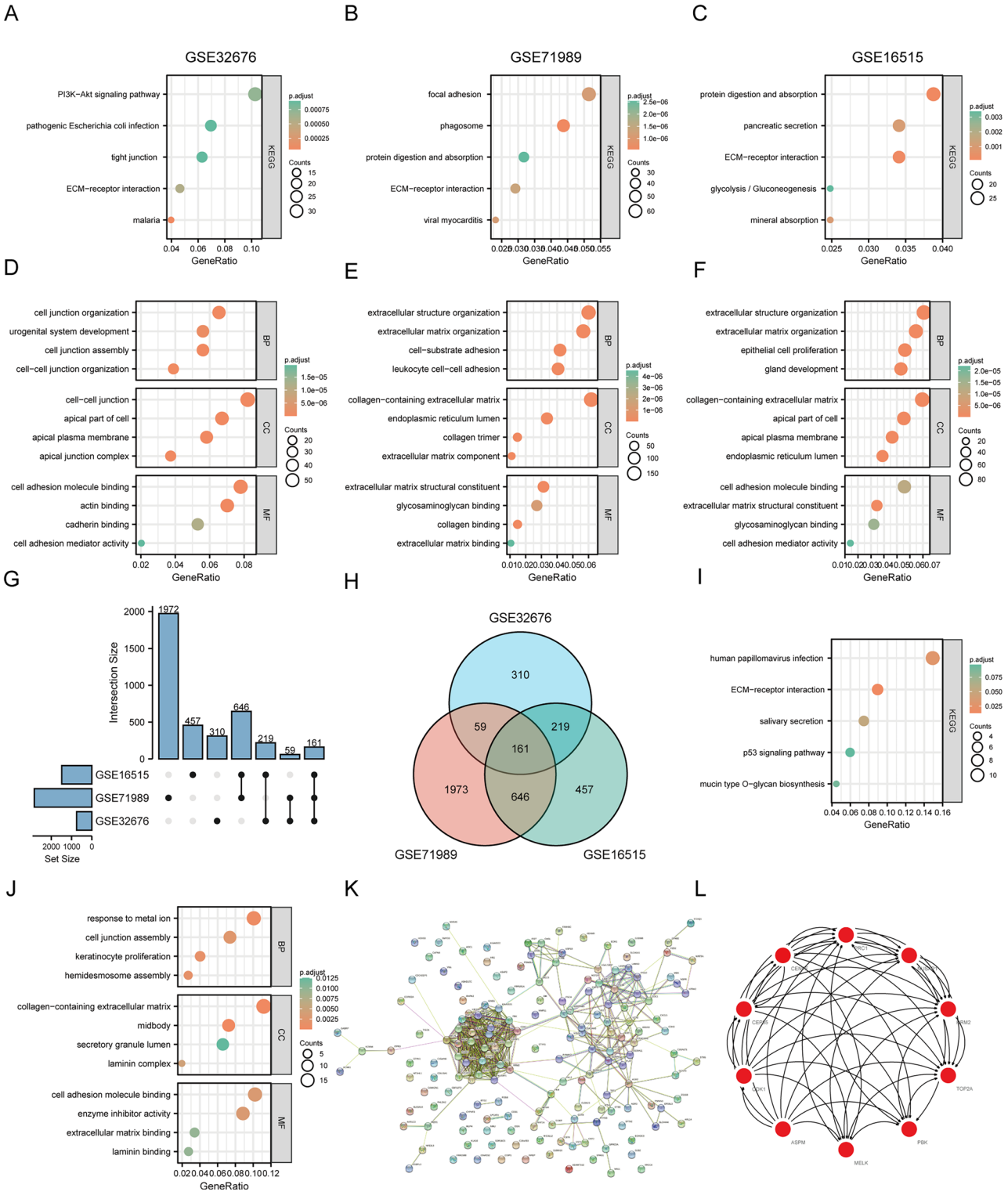

Fig. 2. Functional enrichment of DEGs in pancreatic cancer from GSE32676, GSE71989, and GSE16515 datasets. (**A–C**) The top five enriched KEGG pathways identified for DEGs in pancreatic cancer across the three datasets. (**D–F**) Bubble plots illustrating the top four GO terms categorized under BP, CC, and MF for DEGs identified from the datasets. (**G, H**) The UpSet plot (**G**) and Venn diagram (**H**) depicting the overlapping DEGs in pancreatic cancer. (**I, J**) Enrichment analysis of the overlapping DEGs for KEGG pathways (**I**) and GO terms (**J**). (**K, L**) Identification of the protein-protein interaction (PPI) network (**K**) and the top 10 hub genes (**L**) derived from the overlapping DEGs. KEGG, kyoto encyclopedia of genes and genomes; GO, gene ontology; BP, biological process; CC, cellular component; MF, molecular function.

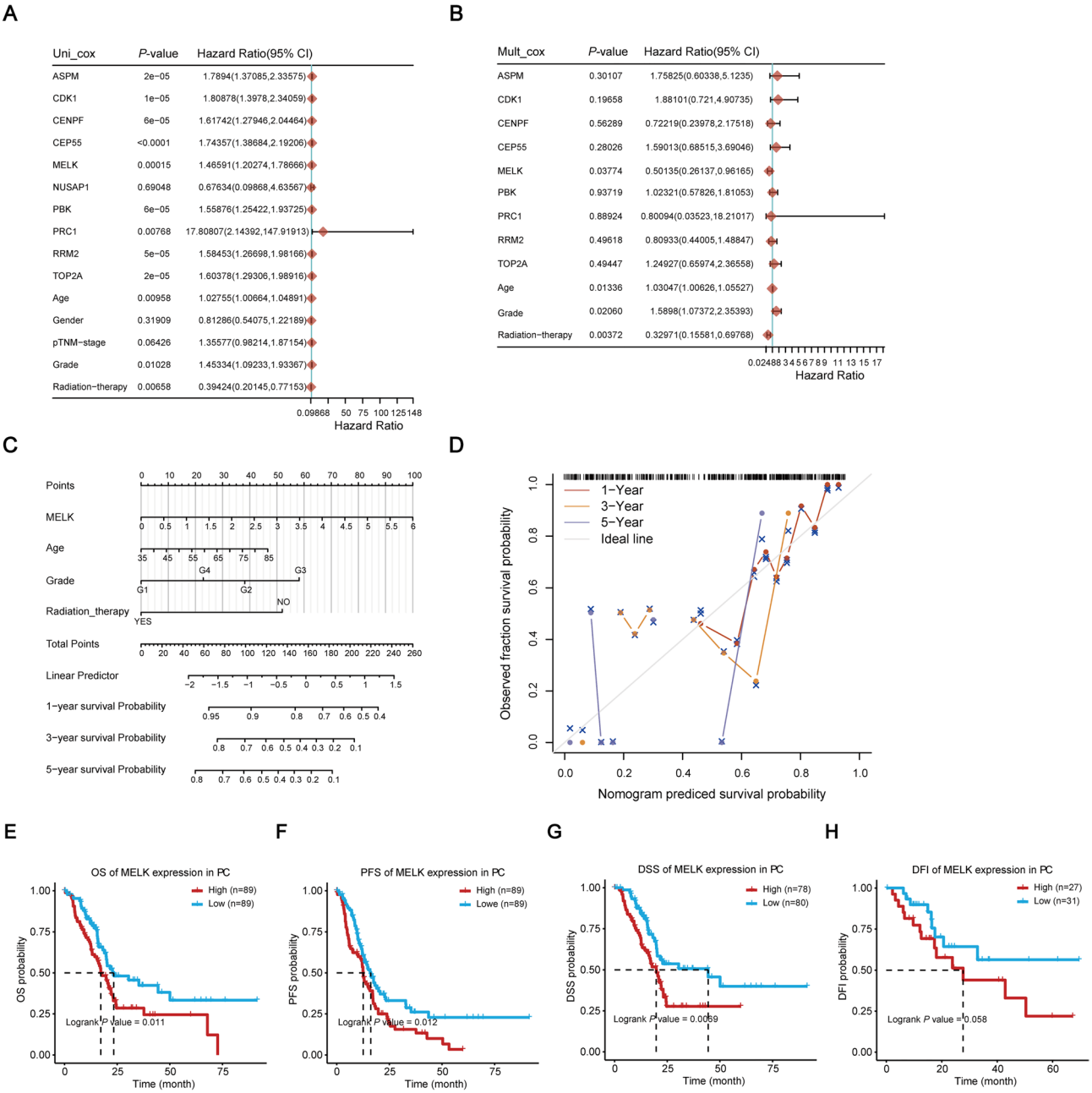

Fig. 3. MELK is positive associated with poor prognosis of patients with pancreatic cancer. (**A, B**) Cox proportional hazards regression analysis was employed to evaluate the association between risk factors and overall survival (OS) in univariate (**A**) and multivariate (**B**) analyses. (**C**) A nomogram was constructed based on MELK expression, age, tumor grade, and radiation therapy. (**D**) Calibration curves for 1-, 3-, and 5-year OS in pancreatic cancer patients demonstrate the model's predictive accuracy. (**E-H**) Elevated MELK expression is significantly associated with worse outcomes in OS, PFS, DSS, and DFI among patients with pancreatic cancer. OS, overall survival; PFS, progression-free survival; DSS, disease-specific survival; DFI, disease-free interval.

MELK serves as an oncogene and promotes cell proliferation, metastasis, and angiogenesis in pancreas cancer

Tumor cell proliferation and metastasis are critical processes for tumor progression in malignant cancers. To further investigate the potential effects of MELK on tumor progression in pancreatic cancer, we overexpressed MELK in the PANC-1 and AsPC-1 pancreatic cell lines. Western blot analyses confirmed the successful overexpression of MELK in both cell lines ($P < 0.01$, Fig. 5A). As anticipated, CCK-8 assays revealed that MELK overexpression significantly promoted cell proliferation in PANC-1 and AsPC-1 cells ($P < 0.0001$, Fig. 5B). Furthermore, compared to the vector control (VC), EdU assay demonstrated a significant enhancement in cell proliferation in the MELK-overexpressing group (MELK-OE) in both pancreatic cell lines ($P < 0.0001$, Fig. 5C). Consistent results were obtained using the colony formation assays, which also showed a remarkable increase

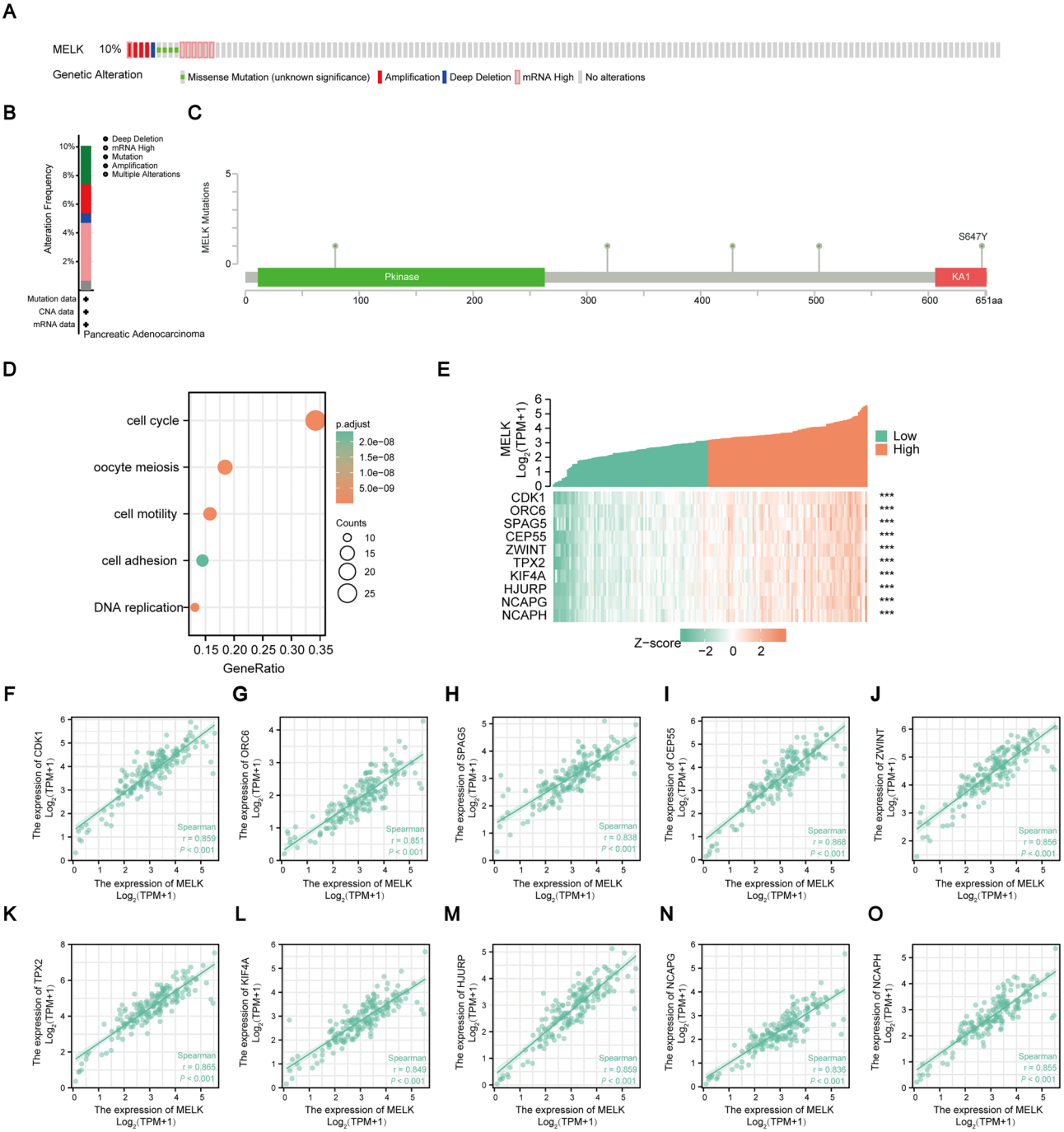

Fig. 4. Mutation feature of *MELK* gene in pancreatic cancer. (**A, B**) Mutation types (**A**) and alteration frequencies (**B**) of the MELK gene in pancreatic cancer. (**C**) Mutation sites of the MELK gene in pancreatic cancer. (**D**) GO enrichment analyses of differentially expressed genes (DEGs) influenced by aberrant MELK expression in pancreatic cancer. (**E**) The top 10 DEGs identified in pancreatic cancer patients exhibiting aberrant MELK expression ($n = 183$) based on data from the TCGA database. (**F-O**) Correlation analyses between MELK expression and the top 10 DEGs in pancreatic cancer patients from the TCGA database.

in cell colonies ($P < 0.0001$, Fig. 5D). These findings indicate that MELK expression plays a significant role in promoting cell proliferation in pancreatic cancer cells. We propose that MELK overexpression may enhance cell proliferation by regulating the cell cycle and DNA replication signaling pathways in pancreatic cancer (Fig. 4D).

We next investigated the role of MELK in tumor metastasis in pancreatic cancer. Transwell assays were conducted to assess the metastatic potential in MELK-overexpressing (MELK-OE) cells compared to the vector control (VC) group. The results revealed that MELK overexpression significantly enhanced tumor metastasis in PANC-1 and AsPC-1 pancreatic cancer cells ($P < 0.01$, Fig. 5E and F). These findings indicate that MELK overexpression is positively correlated with increased tumor metastasis in pancreatic cells. This is consistent

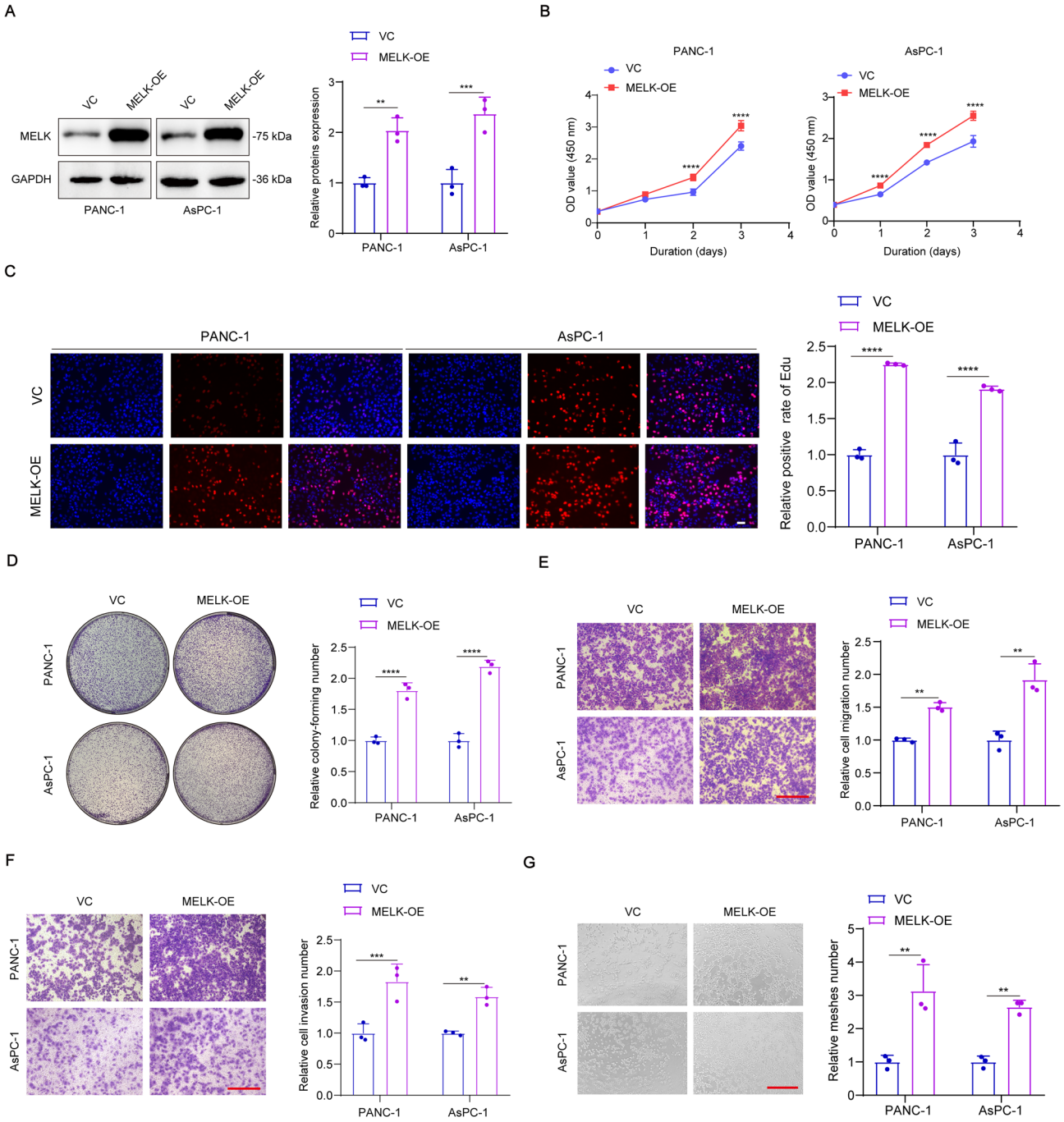

Fig. 5. MELK expression is positively correlate with cell proliferation, tumor metastasis, and angiogenesis in pancreatic cancer cells. (**A**) Analysis and quantification of MELK overexpression and knockdown in PANC-1 and AsPC-1 pancreatic cancer cell lines. (**B**) CCK-8 assays demonstrating increased cell proliferation in MELK-overexpressing PANC-1 and AsPC-1 cells. (**C**, **D**) Representative images and quantification results from the EdU assay (**C**) and colony formation assay (**D**) comparing MELK-overexpressing groups and control groups in PANC-1 and AsPC-1 cells. Scale bar, 200 μm. (E, F) Evaluation of MELK's impact on tumor migration (**E**) and invasion (**F**) in pancreatic cancer cells. Scale bar, 200 μm. (**G**) Tube formation assay illustrating the positive correlation between MELK overexpression and enhanced angiogenesis in pancreatic cancer cells. Scale bar, 200 μm. Data were expressed as mean ± SEM. $^{**}P < 0.01$, $^{***}P < 0.001$, $^{****}P < 0.0001$. VC, vector control; MELK-OE, MELK overexpression.

with the observation that differentially expressed genes (DEGs) associated with aberrant MELK expression in pancreatic cancer are enriched in pathways related to cell motility (Fig. 4D).

Tumor-induced angiogenesis is widely recognized as a critical factor in tumor progression. Based on this, we hypothesized that MELK likely contributes to the regulation of angiogenesis in pancreatic cancer. To investigate

this, we examined the impact of MELK on the angiogenic capacity of pancreatic cancer cells. Surprisingly, the tube formation assay revealed that MELK overexpression significantly enhances angiogenesis in PANC-1 and AsPC-1 cells ($P < 0.01$, Fig. 5G). These findings underscore the pivotal role of MELK in various biological processes associated with pancreatic cancer.

MiR-485-3p directly targets the MELK-3'UTR binding site in pancreatic cancer cells

It is well established that microRNA (miRNA), which regulates the expression of target genes by preventing mRNA transcript degradation and/or inhibiting translation, plays a critical role in tumorigenesis, as well as tumor progression and aggressiveness[24–26]. Using the TargetScan, miRDB, and miRWalk databases, we predicted the potential miRNAs targeting MELK and identified eight candidate miRNAs that overlapped across these three databases (Fig. 6A). Subsequently, we reconstructed the regulatory networks of miRNA–MELK interactions (Fig. 6B). Upon analyzing the expression levels of these miRNAs in pancreatic cancer tissues compared to adjacent normal tissues, the results revealed that only miR-485-3p exhibited a significantly lower expression in pancreatic cancer tissues (Fig. 6C, Supplementary Fig. 3). This finding suggests that miR-485-3p may be associated with MELK-mediated tumor progression in pancreatic cancer. Notably, an analysis of the correlation

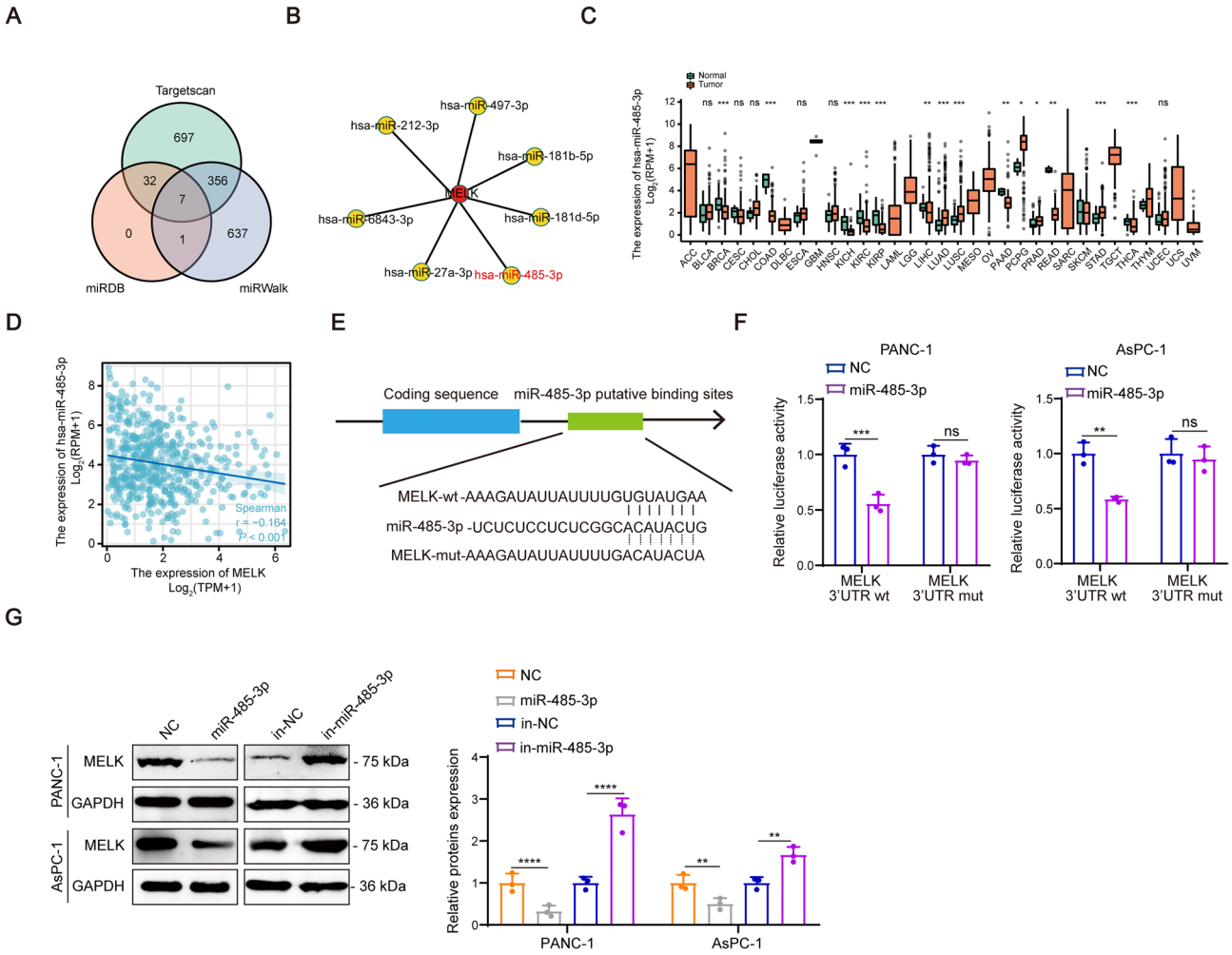

Fig. 6. MiR-485-3p regulates MELK expression by directly targeting the *MELK-3'UTR* binding site in pancreatic cancer cells. (**A**) Prediction of potential miRNAs targeting the MELK gene using the TargetScan, miRWalk, and miRDB databases. (**B**) Regulatory network illustrating the interaction between identified miRNAs and the MELK gene. (**C**) Downregulation of miR-485-3p in pancreatic cancer samples, as observed in the TCGA database. (**D**) Pearson's correlation analysis indicating a negative correlation between miR-485-3p and MELK expression in pancreatic cancer specimens from the TCGA database ($n = 179$). (**E**) Schematic representation of the miR-485-3p binding site, targeting both the wild-type and mutant *MELK 3'UTR* sequences. (**F**) Luciferase assays confirming that miR-485-3p directly targets the *MELK 3'UTR* binding site in pancreatic cancer cells. (**G**) Western blot analysis showing MELK expression after upregulation and downregulation of miR-485-3p in PANC-1 and AsPC-1 cells. $^{**}P < 0.01$, $^{***}P < 0.001$, $^{****}P < 0.0001$, ns, not significant. NC, mimic negative control; miR-485-3p, miR-485-3p mimic; in-NC, inhibitor negative control; in-miR-485-3p, miR-485-3p inhibitor.

between miR-485-3p and MELK expression demonstrated that there was a negative association between miR-485-3p and MELK expression level in pancreatic cancer (Fig. 6D).

To determine whether MELK is a direct target of miR-485-3p, we used the TargetScan database to predict the binding site for miR-485-3p in the *3'UTR* of the *MELK* gene. Figure 6E illustrates a schematic representation of the wild-type (*MELK*-wt) and mutant (*MELK*-mut) binding sites for miR-485-3p within the *3'UTR* sequence of *MELK* gene. A subsequent dual-luciferase reporter assay confirmed that miR-485-3p directly interacts with the binding site in the *3'UTR* sequence of the *MELK* gene ($P < 0.01$, Fig. 6F). Furthermore, overexpression of miR-485-3p (miR-485-3p group) was shown to inhibit MELK expression, whereas reduced levels of miR-485-3p (in-miR-485-3p group) led to an upregulation of MELK expression when compared with their respective negative control groups (NC and in-NC groups) in PANC-1 and AsPC-1 cells ($P < 0.01$, Fig. 6G). These findings strongly support the conclusion that *3'UTR* of *MELK* gene is a direct target of miR-485-3p in pancreatic cancer cells.

miR-485-3p is associated with tumor progression in pancreatic cancer

To investigate the potential role of miR-485-3p in pancreatic cancer cells, we first examined its effect on cell proliferation. Using PANC-1 and AsPC-1 cell lines, miR-485-3p was either overexpressed or inhibited by transfecting the cells with a miRNA mimic or inhibitor. qRT-PCR analysis confirmed that miR-485-3p expression was significantly upregulated in the miR-485-3p mimic group and downregulated in the miR-485-3p inhibitor group in both PANC-1 and AsPC-1 cells ($P < 0.01$, Fig. 7A and B). Subsequent CCK-8 assays revealed that miR-485-3p overexpression markedly suppressed cell proliferation, whereas its knockdown enhanced proliferation in both cell lines ($P < 0.01$, Figs. 7C-F). These findings were further validated through colony formation and EdU assays, which yielded consistent results ($P < 0.01$, Fig. 7G and H).

We then examined the impact of miR-485-3p on tumor metastasis and angiogenesis in pancreatic cancer cells. As anticipated, the Transwell assay demonstrated that overexpression of miR-485-3p significantly inhibited tumor metastasis in both PANC-1 and AsPC-1 cell lines. In contrast, the knockdown of miR-485-3p enhanced tumor metastasis in these cell lines compared to the control groups ($P < 0.05$, Fig. 8A and B). Notably, tube formation assays revealed that the upregulation of miR-485-3p suppressed angiogenic capabilities, while downregulation of miR-485-3p led to the opposite effect in pancreatic cancer cells ($P < 0.05$, Fig. 8C). Furthermore, we assessed the effects of miR-485-3p on proliferation, metastasis, and angiogenesis-related biomarkers. Western blot analyses indicated that overexpression of miR-485-3p markedly decreased the protein expression levels of Cyclin D1, MMP2, MMP9, and VEGFA in PANC-1 and AsPC-1 cells. Conversely, knockdown of miR-485-3p significantly increased the protein levels of these factors in pancreatic cancer cells ($P < 0.05$, Fig. 8D).

MiR-485-3p/MELK cascade mediates tumor progression in pancreatic cancer cells

To investigate the regulatory role of the miR-485-3p/MELK cascade in pancreatic cancer progression, we co-transfected PANC-1 and AsPC-1 cells with MELK siRNA (siMELK group) and/or a miR-485-3p inhibitor (in-miR-485-3p group), along with corresponding negative control groups (in-NC and siNC). Western blot analysis revealed that miR-485-3p downregulation increases MELK expression levels in both PANC-1 and AsPC-1 cells. Notably, suppressing MELK expression counteracted this regulatory effect ($P < 0.01$, Fig. 9A).

To assess the impact of the miR-485-3p/MELK cascade on tumor progression, CCK8 and colony formation assays were employed to evaluate cell proliferation in PANC-1 and AsPC-1 cells ($P < 0.01$, Fig. 9B and C). The data further demonstrated that tumor metastasis was promoted in the in-miR-485-3p group. Conversely, inhibiting MELK expression reversed this effect in both PANC-1 and AsPC-1 cells, highlighting the negative regulatory interplay between MELK and miR-485-3p in pancreatic cancer progression ($P < 0.05$, Fig. 9D and E). Additionally, the effect of the miR-485-3p/MELK cascade on angiogenesis showed consistent findings across PANC-1 and AsPC-1 cells as determined by tube formation assays following treatment with MELK siRNA and/or the miR-485-3p inhibitor ($P < 0.05$, Fig. 9F). Collectively, these results illustrate that miR-485-3p mediates cell proliferation, tumor metastasis, and angiogenesis in pancreatic cancer by modulating MELK expression.

MiR-485-3p/MELK cascade promotes pancreatic cancer progression via Akt signaling pathway

Previous studies have demonstrated that multiple signaling pathways play important roles in the tumorigenesis and tumor progression of pancreatic cancer[27,28]. Our results has indicated that PI3K/Akt/β-catenin signaling pathway might play critical roles in tumorigenesis and development of pancreatic cancer (Fig. 2A). After downregulating miR-485-3p, western blot analyses indicated that phosphorylation of Akt were significantly upregulated ($P < 0.05$), whereas the phosphorylation changes of β-catenin was undetected in PANC-1 and AsPC-1 cells (Fig. 10A). In contrast, miR-485-3p overexpression markedly inhibited activation of Akt signaling pathway in MELK-overexpressing pancreatic cancer cells ($P < 0.001$, Fig. 10B). In addition, the results also indicated that MELK overexpression promoted Akt activation, which was also reversed by capivasertib, a specific Akt inhibitor ($P < 0.05$, Fig. 10C), implying that miR-485-3p/MELK cascade could promote pancreatic cancer progression via Akt signaling pathway.

We then assessed the potential effect of PI3K/Akt signaling pathway in MELK-mediated tumor proliferating, migration and invasion, and angiogenesis in pancreatic cancer. The results showed that MELK overexpression significantly enhanced the abilities of cell proliferation, tumor migration and invasion, and angiogenesis in PANC-1 and AsPC-1 cells, which were subsequently reversed by capivasertib treatment in these process ($P < 0.05$, Fig. 10D-G). Further western blot analyses revealed that MELK overexpression could upregulate the expression levels of Cyclin D1, MMP2, MMP9, and VEGFA, which were the key factors in cell proliferative, tumor invasive and migrative, and angiogenic processes. In contrast, the specific inhibition of PI3K/Akt signaling pathway will block the MELK-regulated expression of Cyclin D1, MMP2, MMP9, and VEGFA in PANC-1 and AsPC-1 cells ($P < 0.05$, Fig. 10H). Together, our findings indicated that MiR-485-3p/MELK cascade promote pancreatic

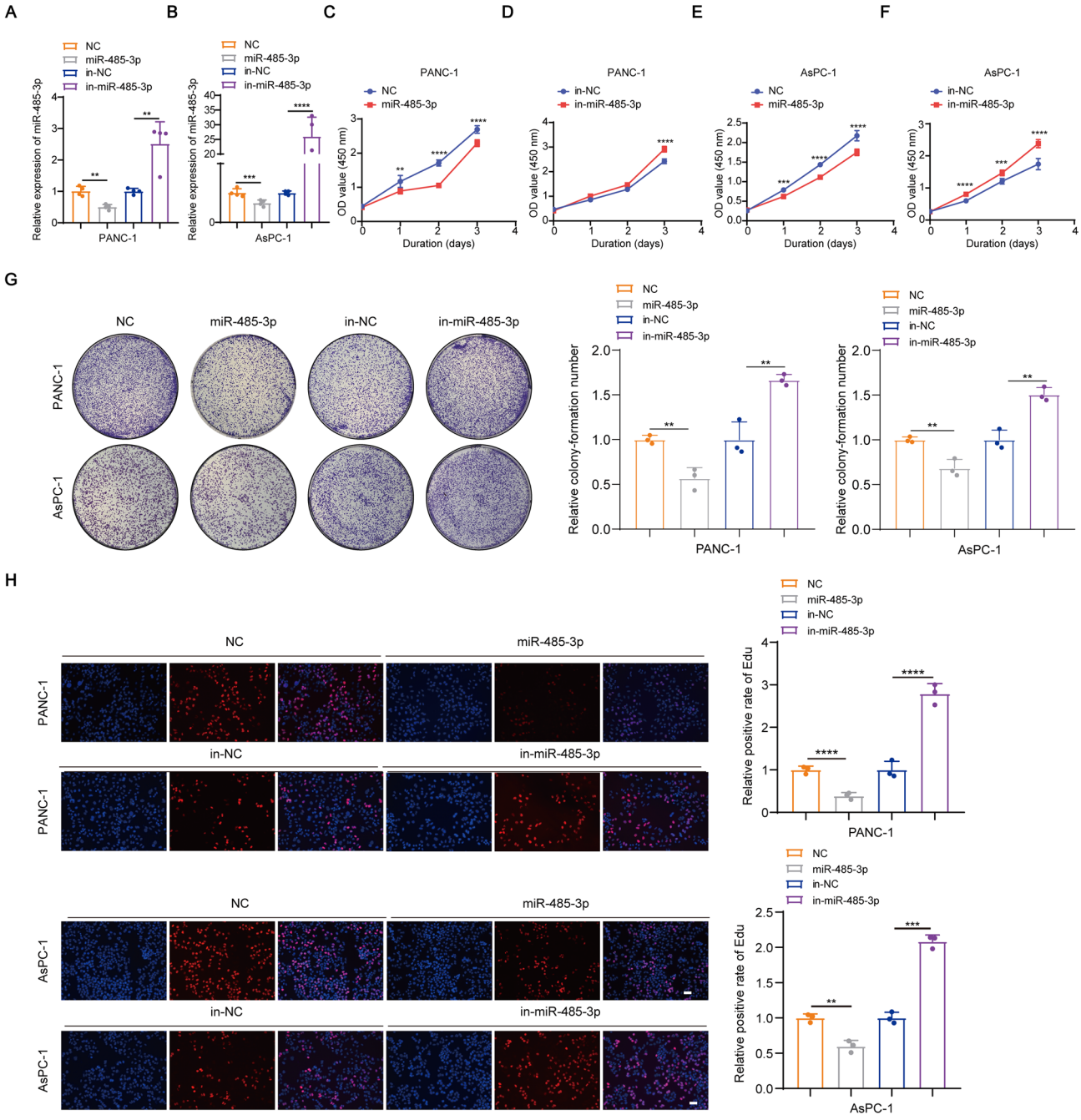

Fig. 7. MiR-485-3p regulates MELK expression to regulate tumor progression in pancreatic cancer. (**A, B**) Measurement of miR-485-3p expression levels following transfection with either the miR-485-3p mimic or inhibitor in PANC-1 (**A**) and AsPC-1 cells (**B**). (**C-F**) Analysis of the impact of miR-485-3p on cell proliferation across various pancreatic cancer cell lines. (**G**) Representative images and quantification of colony formation in pancreatic cancer cells with upregulated or downregulated miR-485-3p expression. (**H**) Representative images and quantification from the EdU assay in pancreatic cancer cell groups exhibiting either upregulated or downregulated miR-485-3p expression. Scale bares, 200 μm. Data were expressed as mean ± SEM. $^{**}P < 0.01$, $^{***}P < 0.001$, $^{****}P < 0.0001$. NC, miR-485-3p mimic negative control; miR-485-3p, miR-485-3p mimic; in-NC, miR-485-3p inhibitor negative control; in-miR-485-3p, miR-485-3p inhibitor.

cancer progression, metastases, and angiogenesis by activating PI3K/Akt signaling pathway in pancreatic cancer cells.

MiR-485-3p/MELK cascade promotes pancreatic tumor growth in vivo

To evaluate the effect of miR-485-3p/MELK on tumor growth in vivo, MELK-overexpressing PANC-1 ($n = 6$) or AsPC-1 cells ($n = 4$) and the control cells were subcutaneously injected into the left forelimb of nude mice, and

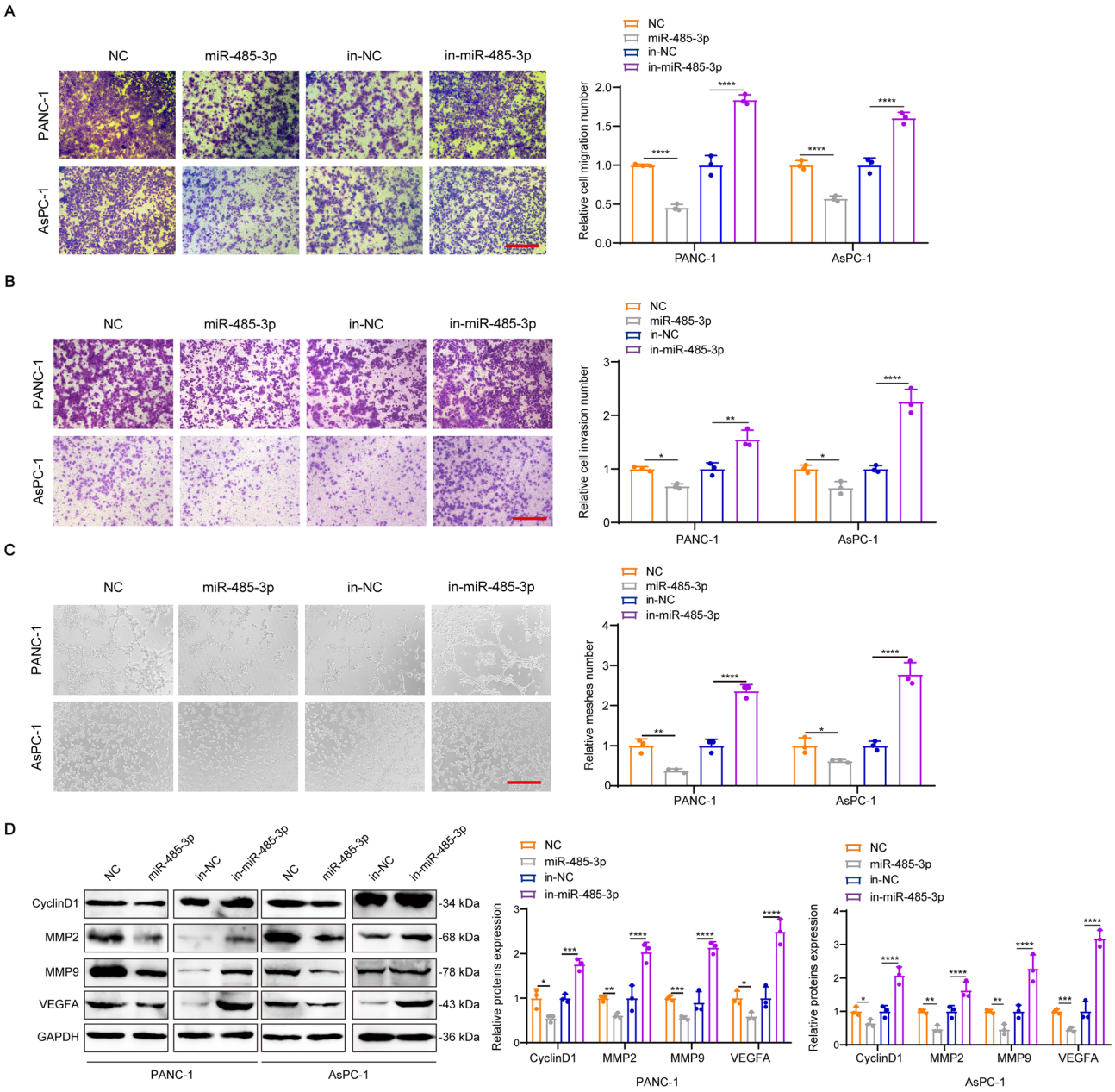

Fig. 8. MiR-485-3p is involved in tumor progression in pancreatic cancer. (**A, B**) Representative images and corresponding quantification illustrating the regulatory effects of miR-485-3p on the migration (**A**) and invasion (**B**) capacities of various pancreatic cancer cell lines. Scale bars, 200 μm. (**C**) Tube formation assays demonstrating the angiogenic potential of pancreatic cancer cells following the upregulation or downregulation of miR-485-3p expression. Scale bars, 200 μm. (**D**) Protein expression levels of cyclin D1, MMP2, MMP9, and VEGFA in PANC-1 and AsPC-1 cells transfected with miR-485-3p mimics, inhibitors, or negative control vectors. Data were expressed as mean ± SEM. $^{*}P<0.05$, $^{**}P<0.01$, $^{***}P<0.001$, $^{****}P<0.0001$. NC, miR-485-3p mimic negative control; miR-485-3p, miR-485-3p mimic; in-NC, miR-485-3p inhibitor negative control; in-miR-485-3p, miR-485-3p inhibitor.

mice were randomly divided into four groups. Thereafter, miR-485-3p agomiR and negative agomiR control were then injected into MELK-overexpressing and control groups, respectively. The results indicated that the tumor growth were significantly enhanced by MELK overexpression, and inhibited by miR-485-3p agomiR treatment, in both PANC-1 and AsPC-1 groups ($P<0.0001$, Figs. 11A-D), indicating that miR-485-3p/MELK cascade is essential for promoting tumor growth in pancreatic cancer. In addition, further western blotting indicated that the expression levels of Cyclin D1, MMP2, MMP9, and VEGFA were upregulated and downregulated in the tumors derived from MELK-overexpressing and miR-485-3p agomiR groups, respectively ($P<0.05$, Fig. 11E).

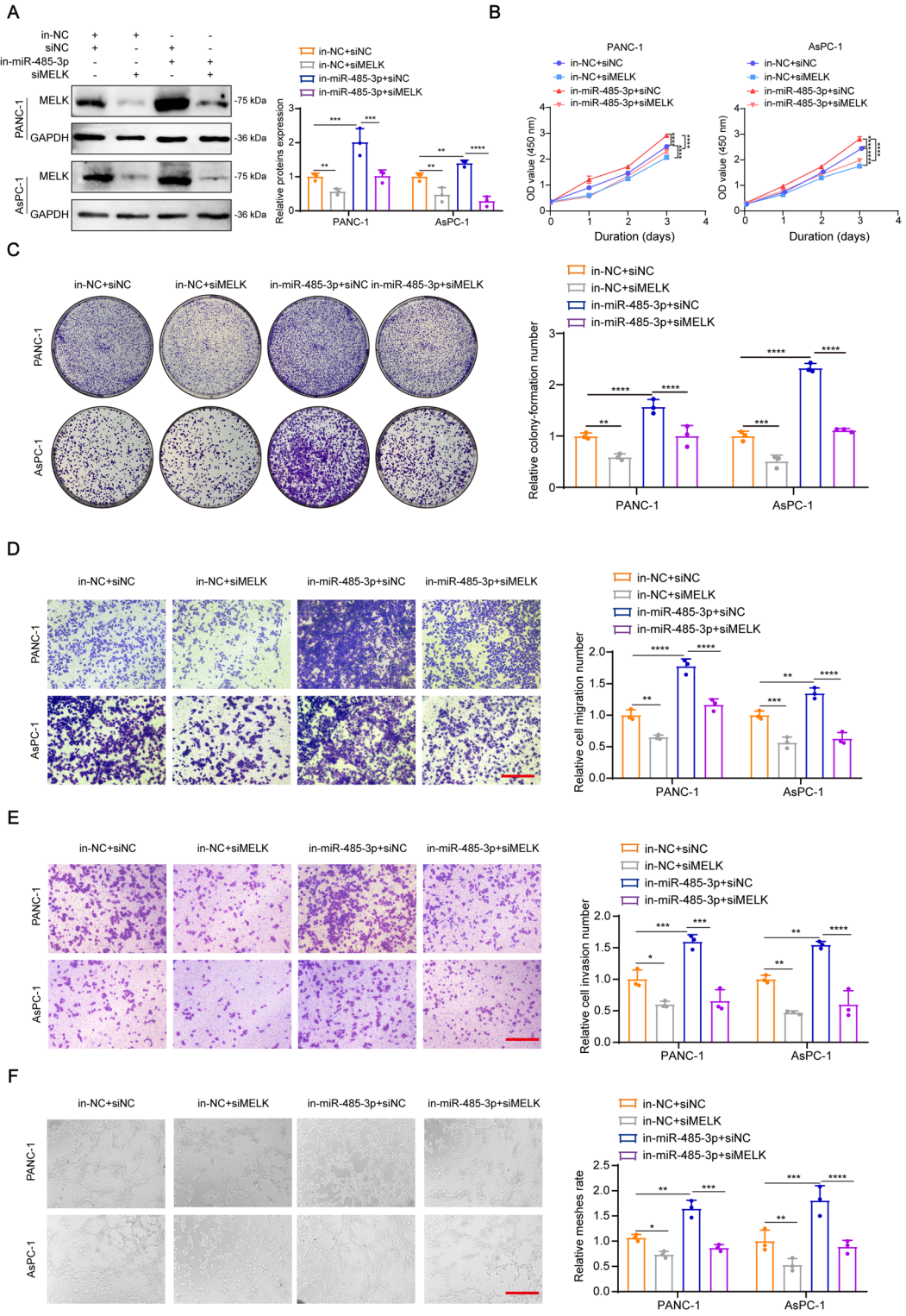

Fig. 9. MiR-485-3p/MELK cascade regulates pancreatic tumor progression. (**A**) Analysis and quantification of MELK expression in PANC-1 and AsPC-1 cells transfected with the miR-485-3p inhibitor (in-miR-485-3p) and/or MELK siRNA (siMELK), alongside their respective negative controls. (**B, C**) The CCK-8 assay (**B**) and colony formation assay (**C**) demonstrate that the miR-485-3p/MELK cascade regulates cell proliferation in various pancreatic cancer cell lines. (**D, E**) Representative images and quantification illustrate the modulation of cell migration (**D**) and invasion (**E**) capabilities, as determined by transwell assays across different groups. Scale bars, 200 μm. (**F**) Representative images and quantitative analysis reveal the angiogenic potential of pancreatic cancer cells transfected with the miR-485-3p inhibitor and/or MELK siRNA. Scale bars, 200 μm. Data were expressed as mean ± SEM. *$P < 0.05$, **$P < 0.01$, ***$P < 0.001$, ****$P < 0.0001$. in-NC, miR-485-3p inhibitor negative control; in-miR-485-3p, miR-485-3p inhibitor; siNC, MELK siRNA negative control; siMELK, MELK siRNA.

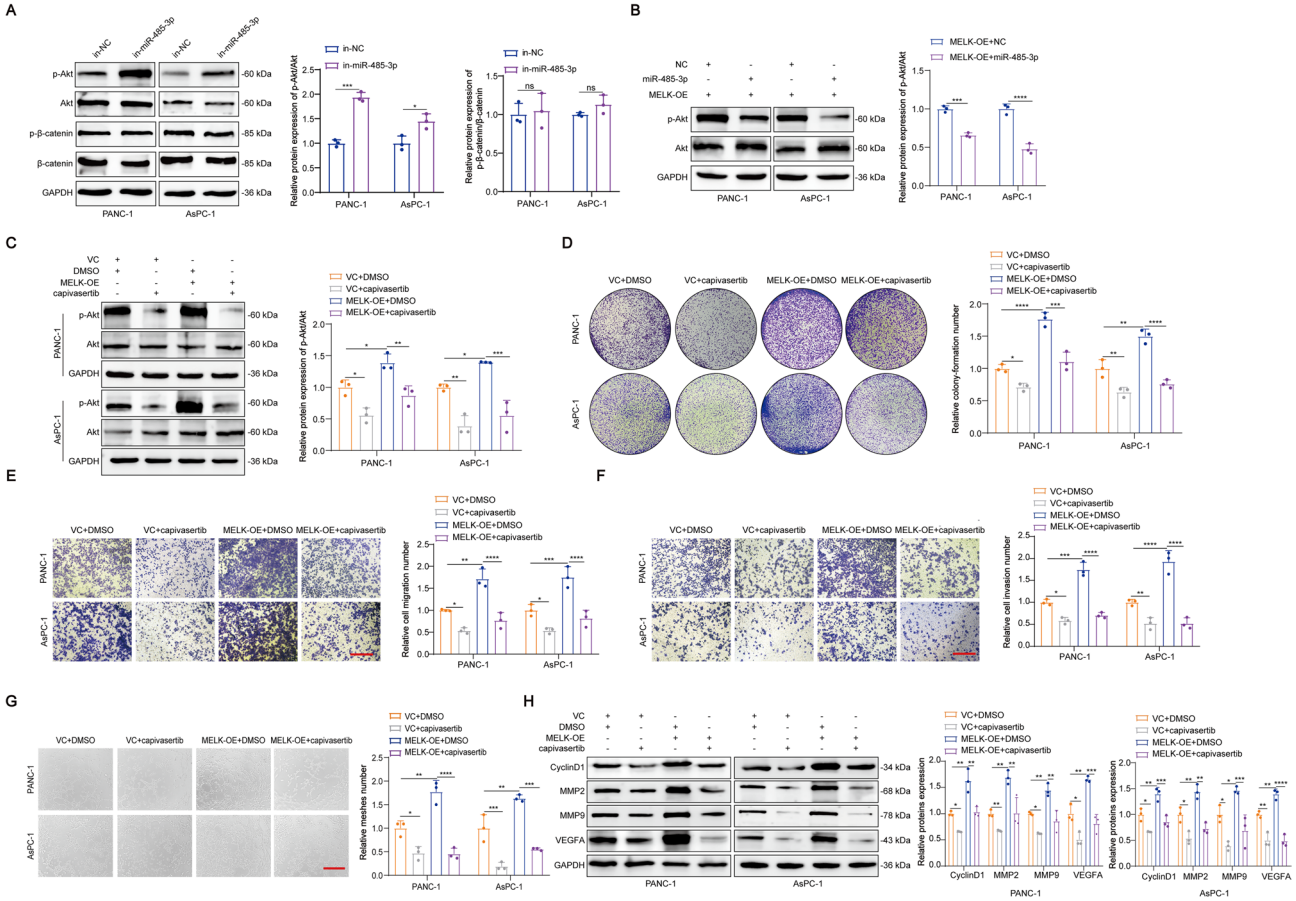

Fig. 10. MiR-485-3p/MELK cascade promotes pancreatic cancer progression via Akt signaling pathway. (**A**) The determination and quantification of the expression levels of phospho-AKt, Akt, phospho-β-catenin, and β-catenin in PANC-1 and AsPC-1 cells with or without transfecting miR-485-3p inhibitors. (**B, C**) The determination and quantification of the expression levels of phospho-Akt and Akt in MELK-overexpressing pancreatic cancer cells transfected with miR-485-3p mimics (**B**) or treated with capivasertib (10 μM) for 48 h (**C**). (**D**) The colony formation in MELK-overexpressing PANC-1 and AsPC-1 cells treated with or without 10 μM capivasertib. (**E, F**) Migration and invasion abilities were evaluated using transwell migration (**E**) and matrigel invasion (**F**) assays in MELK-overexpressing PANC-1 and AsPC-1 cells after treating with 10 μM capivasertib. Scale bars, 200 μm. (**G**) Tube formation assay of MELK-overexpressing pancreatic cancer cells treated with 10 μM capivasertib. Scale bar, 200 μm. (H) The determination and quantification of expression levels of Cyclin D1, MMP2, MMP9, and VEGFA proteins in MELK-overexpressing PANC-1 and AsPC-1 cells treated with or without capivasertib. Data were expressed as mean ± SEM. $^{*}P<0.05$, $^{**}P<0.01$, $^{***}P<0.001$, $^{****}P<0.0001$. in-NC, miR-485-3p inhibitor negative control; in-miR-485-3p, miR-485-3p inhibitor.

Discussion

Despite the identification of potent biomarkers in various malignant cancers, a significant number of malignancies still lack reliable indicators for diagnosis and treatment. Pancreatic cancer, a serious and increasingly prevalent malignancy worldwide, is characterized by a high mortality rate and poor prognosis. At present, diagnostic and prognostic markers for pancreatic cancer patients remain scarce. In this context, the exploration of signaling pathways and key regulators in pancreatic cancer cells may pave the way for developing novel strategies for targeted therapy in its treatment[29]. Certain targeted therapies have shown promising potential in improving the prognosis of patients with pancreatic cancer. For instance, Olaparib, a specific inhibitor of poly(ADP-ribose) polymerase (PARP), has demonstrated significant therapeutic efficacy in metastatic pancreatic cancer associated with BRCA mutations[30]. Additionally, the combination of gemcitabine and the monoclonal antibody nimotuzumab has been shown to effectively enhance outcomes in KRAS wild-type patients with metastatic pancreatic cancer[31]. However, the availability of targeted therapies for pancreatic cancer remains limited, underscoring the need for further advancements in this area.

In this study, we identified 10 critical hub genes - *MELK*, *CEP55*, *NUSAP1*, *ASPM*, *CDK1*, *RRM2*, *TOP2A*, *CENPF*, *PRC1*, and *PBK* - that were highly expressed in pancreatic cancer and associated with poor prognosis (Supplementary Figs. 1, 2 A-J). Notably, most of these hub genes, including *CEP55*, *NUSAP1*, *ASPM*, *RRM2*, *CENPF*, *PRC1*, and *PBK*, were linked to DNA replication[32,33]. Additionally, *CEP55* and *CDK1* were recognized as key factors in cell cycle regulation[34,35]. Our findings further demonstrated that MELK serves as an independent

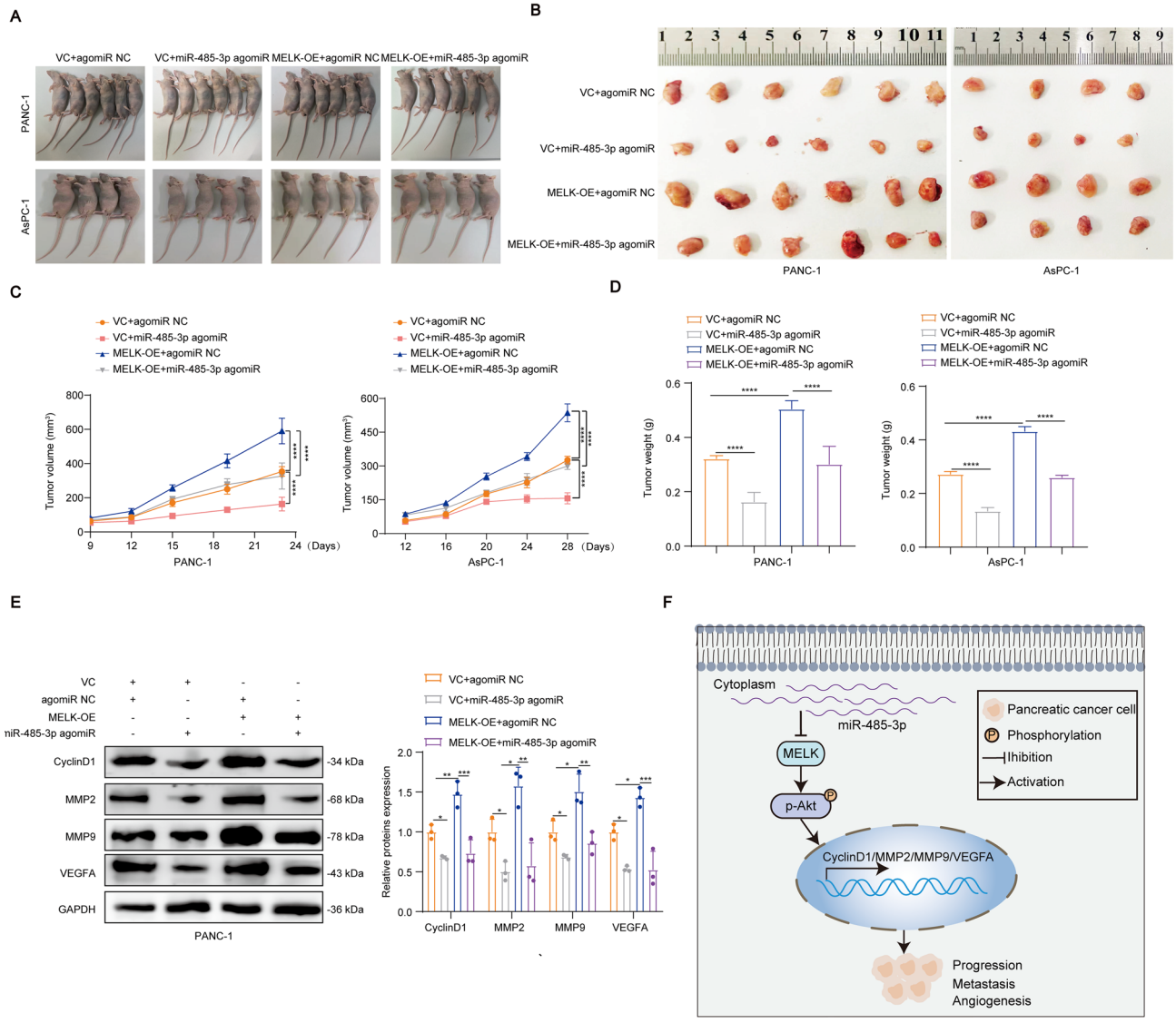

Fig. 11. MiR-485-3p/MELK cascade promotes pancreatic cancer tumor growth in vivo. (**A, B**) Tumor growth is enhanced by MELK overexpression and suppressed by miR-485-3p agomiR treatment in BALB/c-nu mice subcutaneously xenografted PANC-1 ($n = 6$ for each group) and AsPC-1 ($n = 4$ for each group) cells, respectively. (**C, D**) The measurements of tumor volume and tumor weight of the tumors derived from different groups. (**E**) The determination and quantification of the expression levels of Cyclin D1, MMP2, MMP9, and VEGFA proteins in the tumors derived from different groups. (**F**) Schematic of the mechanism by which miR-485-3p/MELK cascade triggers PI3K/Akt signaling pathway and promotes pancreatic cancer progression, metastasis, and angiogenesis. Data were expressed as mean ± SEM. $^{*}P < 0.05$, $^{**}P < 0.01$, $^{***}P < 0.001$, and $^{****}P < 0.0001$.

predictor of prognosis in pancreatic cancer. Previous studies have also shown that MELK is upregulated in various types of tumors and is associated with malignant phenotypes and poor prognoses, lending additional support to our results. The top 10 differentially expressed genes (DEGs) in MELK-overexpressing pancreatic cancer included *CDK1*, *ORC6*, *SPAG5*, *CEP55*, *ZWINT*, *TPX2*, *KIF4A*, *HJURP*, *NCAPG*, and *NCAPH* (Fig. 4E). Furthermore, Gene Ontology (GO) term enrichment analyses revealed that the top five altered downstream signaling pathways were associated with cell cycle regulation, oocyte meiosis, cell motility, cell adhesion, and DNA replication (Fig. 4D). These findings were corroborated by subsequent experimental results. Importantly, *CDK1* and *CEP55* were also identified as key genes in pancreatic cancer in our earlier research (Fig. 2L). CDK1 is well established as the only cyclin-dependent kinase (CDK) essential for cell cycle regulation in mammals[36]. *CEP55*, which encodes the centrosomal protein of 55, was initially identified as a critical regulator of cytokinesis and is overexpressed in multiple types of cancer[37]. Moreover, previous studies have indicated that CEP55 serves as a predictive biomarker for the progression of head and neck squamous cell carcinoma[38]. MELK expression, in turn, has been linked to the simultaneous upregulation of key genes involved in cell cycle progression, such as *CDK1*, *NCAPG*, *CCNB1/2*, and *TOP2A*[39,40]. These studies are consistent with our conclusion that MELK

facilitates tumor progression in pancreatic cancer. Our results further supported the notion that MELK overexpression is essential for pancreatic cancer cell proliferation (Fig. 5B-D). Taken together, we speculate that MELK promotes pancreatic cancer progression by regulating both cell proliferation and cell cycle progression.

We also identified that the downstream effects of MELK overexpression include the cell motility signaling pathway (Fig. 4D), indicating its potential involvement in tumor metastasis. Our experimental results further substantiated this conclusion by demonstrating that MELK overexpression promotes tumor metastasis and angiogenesis in pancreatic cancer cells (Fig. 5E-G). Within this context, the genes listed among the top 10 differentially expressed genes (DEGs) in MELK-overexpressing pancreatic cancer, such as *SPAG5*, *TPX2*, and *KIF4A*, are recognized as key regulators in various malignant cancers. For instance, Li et al. reported that SPAG5 is linked to osteosarcoma metastasis through activation of the FOXM1/MMP2 axis[41]. In non-small cell lung cancer (NSCLC), TPX2 has been shown to drive metastasis and treatment resistance and is considered a biomarker for predicting poor prognosis[42,43]. Similarly, prior studies have revealed that KIF4A overexpression facilitates lymph node metastasis in colorectal cancer[44]. Notably, among these genes, only TPX2 has been identified as a significant angiogenic regulator in various cancers[45–47], suggesting that MELK might induce angiogenesis by regulating TPX2 expression in pancreatic cancer cells. Collectively, these findings indicate that MELK regulates multiple downstream signaling pathways to drive pancreatic cancer progression by promoting cell proliferation, metastasis, and angiogenesis. Nonetheless, the comprehensive regulatory mechanisms underlying MELK-mediated tumor progression in pancreatic cancer require further investigation.

MiR-485-3p has been identified as a tumor suppressor in various cancer types, playing a critical role in tumorigenesis and progression. The primary mechanism of miRNA function involves binding to the *3' UTR* of specific mRNA targets, leading to either mRNA degradation or translational inhibition. Previous reports indicated that the regulation of miR-485-3p is highly complicated, which was involved in ceRNA networks and multi-target interactions. In this context, recent study illustrated that miR-485-3p could inhibit osteosarcoma glycolysis and metastasis by directly suppressing c-MET and AKT3/mTOR signalling[48]. In breast cancer, miR-485-3p plays an important role in the regulation of cell colony formation, migration, and invasion and triggered apoptosis through suppressing by circ-DNMT1[49]. Moreover, recent study demonstrated that overexpression of miR-485-3p suppresses breast cancer cell migration and invasion[50]. Additionally, other studies have shown that miR-485-3p inhibits cell proliferation, colony formation, migration, and sphere formation by specifically binding to the *3'UTR* of *CtBP1*, thereby downregulating its expression[51]. In our research, we observed that miR-485-3p directly interacts with the 3' UTR of MELK, effectively inhibiting its expression. Furthermore, our findings reveal that miR-485-3p/MELK cascade significantly regulates tumor growth, migration and invasion, and angiogenesis by activating PI3K/Akt signaling pathway in PANC-1 and AsPC-1 cells. These results suggest that the miR-485-3p/MELK cascade could serve as a novel therapeutic biomarker for pancreatic cancer.

In summary, MELK has been identified as a potential prognostic biomarker in pancreatic cancer through its influence on multiple pathways, including cell cycle regulation, DNA replication, cell motility, and cell adhesion. This conclusion was reached using an integrated approach combining bioinformatics and experimental characterization. Mechanistically, our results revealed that miR-485-3p directly targets 3'UTR of *MELK* gene to inhibit Akt signaling pathway, thereby suppressing the proliferation, metastasis, angiogenesis and tumor growth in pancreatic cancer cells (Fig. 11F). These findings suggest that the miR-485-3p/MELK cascade could serve as a novel therapeutic target for pancreatic cancer.

Conclusions

We identified ten hub genes, including *MELK*, *CEP55*, *NUSAP1*, *ASPM*, *CDK1*, *RRM2*, *TOP2A*, *CENPF*, *PRC1*, and *PBK*, that play pivotal roles in the progression of pancreatic tumors, based on findings from public databases and clinical data. Further analyses revealed that MELK serves as an independent prognostic marker for pancreatic cancer. The downstream signaling pathways associated with MELK overexpression in pancreatic cancer were primarily linked to cell cycle regulation, DNA replication, and cell motility. Mechanistically, our study identified miR-485-3p as an upstream regulator of MELK, which binds directly to the 3'UTR region of MELK. In addition, miR-485-3p/MELK cascade promotes tumor growth, metastases, and angiogenesis by activating PI3K/Akt signaling pathway. This regulation influences tumor progression by inhibiting proliferation, metastasis, and angiogenesis in pancreatic cancer cells.

Data availability

Data is provided within the manuscript or supplementary information files.

Received: 28 December 2024; Accepted: 14 May 2025
Published online: 22 May 2025

References

1. Gemenetzis, G. et al. Survival in locally advanced pancreatic cancer after neoadjuvant therapy and surgical resection. *Ann. Surg.* **270**, 340–347 (2019).
2. Bray, F. et al. Global cancer statistics 2022: GLOBOCAN estimates of incidence and mortality worldwide for 36 cancers in 185 countries. *CA Cancer J. Clin.* **74**, 229–263 (2024).
3. Klein, A. P. Pancreatic cancer epidemiology: Understanding the role of lifestyle and inherited risk factors. *Nat. Rev. Gastroenterol. Hepatol.* **18**, 493–502 (2021).
4. McGuigan, A. et al. Pancreatic cancer: a review of clinical diagnosis, epidemiology, treatment and outcomes. *World J. Gastroenterol.* **24**, 4846–4861 (2018).
5. Heyer, B. S. et al. New member of the Snf1/AMPK kinase family, Melk, is expressed in the mouse egg and preimplantation embryo. *Mol. Reprod. Dev.* **47**, 148–156 (1997).
6. Tassan, J. P. & Goff, X. L. An overview of the KIN1/PAR-1/MARK kinase family. *Biol. Cell.* **96**, 193–199 (2004).

7. Blot, J. et al. Cell cycle regulation of pEg3, a new Xenopus protein kinase of the KIN1/PAR-1/MARK family. *Dev. Biol.* **241**, 327–338 (2002).
8. Lin, M. L. et al. Involvement of maternal embryonic leucine zipper kinase (MELK) in mammary carcinogenesis through interaction with Bcl-G, a pro-apoptotic member of the Bcl-2 family. *Breast Cancer Res.* **9**, R17 (2007).
9. Kuner, R. et al. The maternal embryonic leucine zipper kinase (MELK) is upregulated in high-grade prostate cancer. *J. Mol. Med. (Berl)*. **91**, 237–248 (2013).
10. Du, T. et al. Maternal embryonic leucine zipper kinase enhances gastric cancer progression via the FAK/Paxillin pathway. *Mol. Cancer*. **13**, 100 (2014).
11. Wang, J. et al. Maternal embryonic leucine zipper kinase: a novel biomarker and potential therapeutic target of cervical cancer. *Cancer Med*. **7**, 5665–5678 (2018).
12. Gray, D. et al. Maternal embryonic leucine zipper kinase/murine protein serine-threonine kinase 38 is a promising therapeutic target for multiple cancers. *Cancer Res.* **65**, 9751–9761 (2005).
13. Zhang, D. & Jiang, P. Maternal embryonic leucine zipper kinase (MELK): a novel regulator in cell cycle control, embryonic development, and cancer. *Int. J. Mol. Sci.* **14**, 21551–21560 (2013).
14. Chen, L. et al. Maternal embryonic leucine zipper kinase promotes tumor growth and metastasis via stimulating FOXM1 signaling in esophageal squamous cell carcinoma. *Front. Oncol.* **10**, 10 (2020).
15. Wang, K., Zhu, X. & Yin, Y. Maslinic acid enhances docetaxel response in human docetaxel-resistant triple negative breast carcinoma MDA-MB-231 cells via regulating MELK-FOXM1-ABCB1 signaling cascade. *Front. Pharmacol.* **11**, 835 (2020).
16. Nishitoh, H. et al. ASK1 is essential for JNK/SAPK activation by TRAF2. *Mol. Cell.* **2**, 389–395 (1998).
17. Seong, H. A. & Ha, H. Murine protein serine-threonine kinase 38 activates P53 function through Ser15 phosphorylation. *J. Biol. Chem.* **287**, 20797–20810 (2012).
18. Edgar, R., Domrachev, M. & Lash, A. E. Gene expression omnibus: NCBI gene expression and hybridization array data repository. *Nucleic Acid Res.* **30**, 207–210 (2002).
19. Kanehisa, M. et al. KEGG: biological systems database as a model of the real world. *Nucleic Acids Res.* **53**, D672–D677 (2025).
20. Kanehisa, M. Toward Understanding the origin and evolution of cellular organisms. *Protein Sci.* **28**, 1947–1951 (2019).
21. Kanehisa, M. & Goto, S. KEGG: Kyoto encyclopedia of genes and genomes. *Nucleic Acids Res.* **28**, 27–30 (2000).
22. Szklarczyk, D. et al. STRING v10: protein-protein interaction networks, integrated over the tree of life. *Nucleic Acid Res.* **43**, D447–D452 (2015).
23. Cerami, E. et al. The cBio cancer genomics portal: an open platform for exploring multidimensional cancer genomics data. *Cancer Discov*. **2**, 401–404 (2012).
24. Rupaimoole, R. & Slack, F. J. MicroRNA therapeutics: towards a new era for the managment of cancer Anc other diseases. *Nat. Rev. Drug Discov*. **16**, 203–222 (2017).
25. Jansson, M. D. & Lund, A. H. MicroRNA and cancer. *Mol. Oncol.* **6**, 590–610 (2012).
26. Budakoti, M. et al. *Micro-RNA: Darkhorse cancer* ;**83**:109995. (2021).
27. Zhuo, F. et al. The role of signaling pathways in pancreatic Cancer targeted therapy. *Am. J. Clin. Oncol.* **46**, 121–128 (2023).
28. Wu, B. et al. Downregulation of Smurf2 ubiquitin ligase in pancreatic cancer cells reversed TGF-β-induced tumor formation. *Tumour Biol.* **37**, 16077–16091 (2016).
29. Park, W., Chawla, A. & O'Reilly, E. M. Pancreatic cancer: a review. *JAMA* **326**, 851–862 (2021).
30. Golan, T. et al. Maintenance Olaparib for germline BRCA-mutanted metastatic pancreatic cancer.
31. Schultheis, B. et al. Gemcitabine combined with the monoclonal antibody nimotuzumab is an active first-line regimen in KRAS wildtype patients with locally advanced or metastatic pancreatic cancer: a multicenter, randomized phase IIb stidy. *Ann. Oncol.* **28**, 2429–2435 (2017).
32. Wang, G. et al. CEP55 as a promising immune intervention marker to regulate tumor progression: a pan-cancer analysis with experimental verification. *Cells* **12**, 2457 (2023).
33. Han, Z. et al. PBK/TOPK: a therapeutic target worthy of attention. *Cells* **10**, 371 (2021).
34. Xu, Z. Y. et al. Cep55 regulates spindle organization and cell cycle progression in meiotic oocyte. *Sci. Rep.* **5**, 16978 (2015).
35. Wang, Q., Bode, A. M. & Zhang, T. Targeting CDK1 in cancer: mechanisms and implications. *NPJ Precis Oncol.* **7**, 58 (2023).
36. Santamaría, D. et al. Cdk1 is sufficient to drive the mammalian cell cycle. *Nature* **448**, 811–815 (2007).
37. Jeffery, J. et al. Beyond cytokinesis: the emerging roles of CEP55 in tumorigenesis. *Oncogene* **35**, 683–690 (2016).
38. Waseem, A. et al. Downstream targets of FOXM1: CEP55 and HELLS are cancer progression marker of head and neck squamous cell carcinoma. *Oral Oncol.* **46**, 536–542 (2010).
39. Goto, Y. et al. Impact of novel miR-145-3p regulatory networks on survival in patients with castration-resistant prostate cancer. *Br. J. Cancer*. **117**, 409–420 (2017).
40. Chen, H. et al. Bioinformatics analysis of key genes and pathways of cervical cancer. *Onco Targets Ther.* **13**, 13275 (2020).
41. Li, Z. et al. SPAG5 promotes osteosarcoma metastasis via activation of FOXM1/MMP2 axis. *Int. J. Biochem. Cell. Biol.* **126**, 105797 (2020).
42. Hu, J. et al. Transmission of Exosomal TPX2 promotes metastasis and resistance of NSCLC cells to docetaxel. *Onco Targets Ther.* **16**, 197–210 (2023).
43. Zhou, F. et al. TPX2 promotes metastasis and serves as a marker of poor prognosis in non-small cell lung cancer. *Med. Sci. Monit.* **26**, e925147 (2020).
44. Matsumoto, Y. et al. Enhanced expression KIF4A in colorectal cancer is associated with lymph node metastasis. *Oncol. Lett.* **15**, 2188–2194 (2018).
45. Li, X. Q. et al. E2F8-TPX2 axis regulates Glycolysis and angiogenesis to promote progression and reduce chemosensitivity of liver cancer. *Cytotechenology* **76**, 817–832 (2024).
46. Wang, T., Zhang, F. & Zhang, P. Role of the TPX2/NCOA5 axis in regulating proliferation, migration, invasion and angiogenesis of breast cancer cells. *Exp. Ther. Med.* **25**, 304 (2023).
47. Li, X. et al. Secretory autophagy-induced bladder tumour-derived extracellular vesicle secretion promotes angiogenesis by activating the TPX2-mediated phosphorylation of the AURKA-PI3K-AKT axis. *Cancer Lett.* **523**, 10–28 (2021).
48. Wang, Q. et al. miR-485-3p regulated by MALAT1 inhibits osteosarcoma Glycolysis and metastasis by directly suppressing c-MET and AKT3/mTOR signalling. *Life Sci.* **268**, 118925 (2021).
49. Xie, C. et al. CircRNA DNA methyltransferase 1 silence inhibits breast cancer development by regulating micoRNA-485-3p/zinc finger E-box binding homeobox 1 axis. *J. Obstet. Gynaecol. Res.* **47**, 1068–1081 (2021).
50. Lou, C. et al. MiR-485-3p and miR-485-5p suppress breast cancer cell metastasis by inhibiting PGC-1α expression. *Cell. Death Dis.* **7**, e2159 (2016).
51. Du, K. et al. MicroRNA485-3p negatively regulates the transcriptional co-repressor CtBP1 to control the oncogenic process in osteosarcoma cells. *Int. J. Biol. Sci.* **14**, 1445 (2018).

Acknowledgements

This work was supported by the National Natural Science Foundation of China (81872070), the Guangxi National Science Foundation for Guangdong - Guangxi United Program (2021GXNSFDA075014), and the Natural Science Foundation of Guangdong Province (2022A1515012424 and 2023A1515011749).

Author contributions

Y.H. collected data, participated in the design of the study, and performed experiments, data analysis, and manuscript writing. T.Y. and Y.C. contributed to data analysis and discussion. B.T. reviewed and revised the manuscript. B.S. supervised, reviewed and revised the manuscript. X.Y. supervised, obtained funding, reviewed and revised the manuscript. All authors reviewed the manuscript.

Declarations

Competing interests

The authors declare no competing interests.

Conflict of interest

The authors have no conflicts of interest to declare.

Additional information

Supplementary Information The online version contains supplementary material available at https://doi.org/10.1038/s41598-025-02586-8.

Correspondence and requests for materials should be addressed to B.S. or X.Y.

Reprints and permissions information is available at www.nature.com/reprints.

Publisher's note Springer Nature remains neutral with regard to jurisdictional claims in published maps and institutional affiliations.